Synthesis of clean hydrogen gas from waste plastic at zero net cost

Kevin M. Wyss[1], Karla J. Silva[1], Ksenia V Bets[2], Wala A. Algozeeb[1], Carter Kittrell[1], Carolyn H. Teng[1], ChiHun Choi[1], Weiyin Chen[1], Jacob Beckham[1], Boris I. Yakobson,[1,2,3,*] and James M. Tour[1,2,3,*]

[1]Department of Chemistry, Rice University, Houston, TX 77005, USA

[2]Department of Materials Science and NanoEngineering, Rice University, Houston, TX 77005, USA

[3]Smalley-Curl Institute, NanoCarbon Center and the Rice Advanced Materials Institute, Rice University, Houston, TX 77005, USA

*Corresponding authors. Email: biy@rice.edu; tour@rice.edu

Abstract: Hydrogen gas (H_2) is the primary storable fuel for pollution-free energy production, with over 90 million tonnes used globally per year. More than 95% of H_2 is synthesized through metal-catalyzed steam methane reforming that produces 11 tonnes of CO_2 per tonne H_2. "Green H_2" from water electrolysis using renewable energy produces sub-stoichiometric CO_2, but costs 2-3x more, making it presently economically unviable. Here we report catalyst-free conversion of waste plastic into clean "flash H_2" along with high purity graphene. The scalable procedure evolves no CO_2 when deconstructing polyolefins and produces H_2 in purities up to 94% at high mass yields. Sale of the graphene byproduct at just 5% of its current value yields H_2 production at negative cost. Life-cycle assessment demonstrates a 39-84% reduction in emissions compared to

other H_2 production methods, suggesting the flash H_2 process to be an economically viable, clean H_2 production route.

One-Sentence Summary: Efficient flash Joule heating allows for the catalyst-free deconstruction of waste plastic into clean flash H_2 at zero net cost.

Main Text:

Hydrogen gas (H_2) constitutes an attractive energy technology due to its high-efficiency in fuel cells and greenhouse gas-free combustion. Ironically, however, 95% of global H_2 is produced by steam methane reforming (called "grey hydrogen") which evolves 11 tonnes of CO_2 per 1 tonne of H_2. That singular process is responsible for 800 million tonnes (MT) of CO_2 production annually, equal to the annual CO_2 emissions of the United Kingdom.(*1*) H_2 demand is projected to grow rapidly throughout the next three decades (Figure 1a), so alternative production methods are needed to mitigate further CO_2 emissions.(*2*) Electrolysis of water to produce H_2 ("green hydrogen") and O_2 presents one such pathway, affording little greenhouse gases when powered by renewable energy.(*3*) Disappointingly, despite current emissions-consciousness, electrolysis affords <5% of global H_2 production because of its high cost (Figure 1b)(*4*); expensive metal catalysts, such as Pt, Ir, or Ru, are often required.(*5*) For every 1 tonne of H_2 produced, 9 tonnes of fresh water are consumed, limiting implementation of electrolysis in some locales.(*6*) High temperature methane pyrolysis to form H_2 plus solid carbon ("turquoise hydrogen"), and steam methane reforming with associated CO_2 capture ("blue hydrogen"), do not result in the release of stoichiometric greenhouse gases but they still require fossil-fuel feedstocks and are not yet economically competitive with traditional grey hydrogen.(*7*, *8*)

Ideally, low-cost H_2 production methods are needed that evolve little CO_2, require no costly catalysts, and use abundant feedstocks.(*9*) In 2021, the US Department of Energy targeted the production of 1 kg of H_2 for $1 in 1 decade, the so-called "1:1:1" goal.(*10*) The co-production of H_2 with high-value materials could afford an economic basis to achieve this goal, and thereby displace steam methane reforming (Figure 1c). Concurrently, waste plastics are up to 14 wt% atomic H and are widely available since 380 MT are produced annually, plus there are enormous backlogs of accumulated waste plastics.(*11*) Consequently, several technologies have viewed waste plastic as a source of H_2. Typically, plastic pyrolysis converts waste plastics into small hydrocarbons, which are then steam reformed to yield H_2, CO, and CO_2.(*12*, *13*) These reactions further require complex catalysts. Recent research has demonstrated the use of $FeAlO_x$ with microwaves to degrade polyolefins into H_2, light olefins, and impure carbon nanotubes due to rapid heating rates, but the $FeAlO_x$ is required in equal weight to waste plastic feedstock and the microwave energy input is large.(*14*)

In this work, we show that rapid flash Joule heating (FJH) of waste plastic can be performed with no added catalyst to deconstruct polyolefins, polyesters, and mixed waste plastics, affording high yields of H_2 (that we refer to as "flash H_2") along with high purity graphene as a value-added byproduct. Based on the sale of the graphene byproduct of this flash H_2-production process, the H_2 produced has negative production cost, even if the graphene is sold at <5% (US$3,000 per tonne) of its current market cost of US$60,000-US$100,000 per tonne. Moreover, a life-cycle assessment shows that the FJH of polyolefins produces "clean H_2" as defined by the US Department of Energy by generating <4 kg CO_2 per 1 kg H_2. Flash H_2 uses less energy than green or turquoise H_2, while producing less greenhouse gas emissions than grey, blue, and turquoise H_2. Therefore, this catalyst-free flash H_2 route removes mixed waste plastic streams, upcycling them

into graphene, while generating up to 47 mol of H_2 per kg of input plastic, all at an overall negative cost for this clean H_2 fuel source.

Catalyst-free polyethylene deconstruction optimization

FJH leverages rapid current discharge through a resistive feedstock to achieve heating within the resistor, removing slow heat transfer steps, allowing for heating rates up to 10^5 K s^{-1} and achieving temperatures of ~3,100 K.(*15*, *16*) A general scheme of the methods used here is presented in Figure 2a and Figure S1-2. The resistance of the sample limits the magnitude of current by Ohm's law, controlling the amount of heat generated. Here, capacitors supply the current, but AC voltage sources can also be used.(*17–19*) Plastics are an electrically insulating thus requiring a conductive additive, thereby forming a conductive path between the polymer grains.(*20*) Low (3-5 wt%) amounts of conductive additive, such as carbon black, result in higher resistances, limiting the amount of current discharge and therefore heat generated, while 16 wt% additive results in lower feedstock resistances, higher reaction temperatures, and faster current discharge (Figure 2b).

Iterative current discharges are used to heat the plastic waste sample. The current discharged through the sample can be measured by a Hall effect sensor. Through iterative discharges, the resistance of the sample decreases as the plastic is carbonized, resulting in higher currents and faster discharge. Jagged, interrupted current is observed in the first three discharges due to the outgassing of volatiles momentarily pushing the spring-loaded electrodes apart, intermittently opening the circuit. A smooth fourth current discharge demonstrates no more outgassing (Figure 2a). These volatiles are trapped, then studied by gas chromatography (GC) with thermal conductivity and mass spectrometer (MS) detectors.

The produced volatile streams contain large amounts of H_2, along with other hydrocarbons. Post-consumer high density polyethylene (HDPE) waste was used to optimize the process. Production of H_2 was found to correlate with the initial sample resistance; lower resistances resulting in higher H_2 production. Hydrogen efficiency has previously been defined as the total mass of atomic hydrogen contained in all gas phase products, as compared to the atomic hydrogen content of starting polymer.(*14*) Hotter, faster heating rates result in more H_2 recovered and more atomic hydrogen liberated from solid polymer (Figure 2c), and up to 46.6 mmol H_2 per g of HDPE, 92.7% efficiency, and 87% gas purity are obtained when the initial resistance is 6 Ohm. Other gases are produced, predominantly consisting of methane and short alkenes. As higher temperatures and faster heating rates are reached, the purity of the flash H_2 increases (Figure 2d, bar graph). In an ideal reaction, all carbon atoms in the polyethylene would convert to graphene, while all hydrogen atoms would be released as H_2. The percentage yield *versus* this ideal maximum is also plotted in Figure 2d (line graph).

A complete mass balance is required to understand what other products result from the deconstruction. Figure 2e shows the mass yield of flash H_2, graphene, hydrocarbon gases, oils, waxes, and aromatic residues produced by the FJH deconstruction. Hotter and faster reactions favor more complete polymer deconstruction, resulting in lower hydrocarbon gas, oil, and wax production, with higher graphene and H_2 yields at lower sample resistances.

The carbon atoms left behind by the evolution of H_2 from waste plastic are rearranged into the 2D nanomaterial graphene. Graphene, with its high strength and conductivity, has been studied extensively since its isolation.(*21*, *22*) A multitude of demonstrated graphene applications exist, including composites with concrete, asphalt, and plastics, as well as gas and water filtration, energy storage devices, and flexible electronics, with industrial-scale implementation being realized in 2018 by Ford Motor Company. Graphene is in all Ford automobiles since February 2020,

predominantly in the foam cushion seats and under-hood insulation.(*23–25*) Single- or few-layered graphene sheets have high value due to current worldwide production limitations of only 15 tons per day.(*26*) As the price declines, extensive use is projected in many large-scale construction materials markets.

Low defect content, few-layer composition, and high carbon content are favorable properties for graphene applications.(*27*) Raman spectroscopy is the most common method to characterize graphene since it can inform the quality, layering, and orientation based on major peaks including the D peak at ~1350 cm^{-1} indicating lattice defect content, G peak at ~1600 cm^{-1} indicating sp^2-hybridized character, and 2D peak at ~2690 cm^{-1} indicating graphene sheet layering.(*28*) Since large amounts of graphene nanocrystals are produced with each reaction, large area Raman spectral analysis allows for analysis of 100 different spectra to provide a representative single spectrum with standard deviation and graphene purity determination (Figure 3a-b). Lower feedstock resistances result in better graphene quality, determined by defect content (D peak intensity) and graphene lattice quality (2D peak intensity, shape, position, and width), as well as higher product purity of 97-99% graphene. Since lower resistances result in higher reaction temperatures, more annealed graphene sheets and less amorphous carbon result.

Deconstruction of waste polyethylene can be followed by powder X-ray diffraction (XRD), showing near-complete conversion to graphene over the optimized FJH process (Figure 3c). The powder XRD also shows a broadening of the graphene (002) peak consistent with few-layer graphene, and little detectable residual crystalline impurities.(*29*) Since no catalyst is used and only small amounts of carbon additive are required, the graphene product has high carbon purity and sp^2-hybridization, as probed by X-ray photoelectron spectroscopy, unlike similar plastic deconstruction processes, suggesting that no further purification or processing is required prior to graphene use (Figure 3d). Thermogravimetric analysis also indicates high purity graphene

formation; a single and complete degradation is observed at 680°C under air atmosphere, showing no residual inorganic or polymer content (Figure S3). Large, highly crystalline, sheet-like morphologies of waste plastic derived graphene are observed by scanning electron microscopy imaging (Figure 3e). Transmission electron microscopy demonstrates few-layer thickness and turbostratic stacking (Figure S4).

Exfoliation of graphene and its dispersion are essential considerations in composite, anode, or device fabrication. Turbostratic, or rotationally disordered, layering of graphene sheets disrupts the interlayer π-π interactions providing unique electronic and magnetic properties, and significantly lowering the barrier for graphene sheet exfoliation.(*30*, *31*) Rapid heating and cooling rates kinetically trap the graphene byproduct as turbostratic graphene, apparent through high resolution Raman spectroscopic analysis. The appearance of TS_1 and TS_2 peaks, and the missing M peak signify turbostratic graphene, resulting in superior dispersibility when compared to commercial graphene made by graphite exfoliation, which displays ordered AB-stacking and the expected M peak by Raman analysis (Figure 3f, Figure S5).(*32*)

Graphene formed by the FJH method has been leveraged in many demonstrated applications, including composites, energy storage in Li batteries, and electrocatalysis.(*19*, *29*, *33*) In ~3 years, FJH production of graphene has increased from 1 g per hour to >1 kg per hour rates at laboratory scale, while industry has achieved pilot plant tonne-per-day rates.(*34*) Feedstocks besides waste plastics should also be considered, that are ideally high in atomic H content and low in atomic O content to minimize CO_2 evolution. Asphalt, bitumen, and asphaltenes contain >11% H and <1% O, and they present large-scale, low-cost materials that can supplement plastic deconstruction for H_2 production if necessary.(*35*) Asphaltenes are demonstrated here to also produce high purity H_2 and graphene byproduct (Figure S6).

Process generality of catalyst-free polymer deconstruction

Although polymer recycling methods have existed for decades, 95% of produced plastic is never recycled due to the high cost of manually separating the diverse plastic types, large amounts of hot water and detergent required for washing prior to re-melting, and an inferior recycled polymer product when compared to virgin plastics. Since the flash H_2 process needs no catalyst, we hypothesized that it would proceed similarly with any feedstock. Figure 4a shows that hydrogen efficiency is not substantially impacted by the polymer identity. Since other polymers screened contain less atomic hydrogen than HDPE, it is expected that less H_2 per gram of polymer is recovered. The purity of H_2 resulting from all polyolefins is >84%. Some CO and CO_2 is produced when polyesters are deconstructed, resulting from oxygen present in the ester linkages. Similarly, some N_2 is produced when N-containing polymers such as acrylonitrile-butadiene-styrene (ABS) is deconstructed (Figure 4b).

Mixed waste plastic can be readily deconstructed without any separation or washing. The flash H_2 process achieves 52-68% yields for H_2, and 46-63% yields for graphene for all polymers and mixes studied, outperforming other catalyst-free deconstruction methods by 5-10x. Polystyrene produces the highest purity H_2 stream since the aromatic stability of the styrene minimizes the formation of gaseous hydrocarbons.

Instead of carbon black, lower-value conductive additives were studied to decrease costs upon process scale-up. Waste ash resulting from the pyrolysis of plastics, charcoal, and metallurgical coke (metcoke) were used, and Figure 4c-d shows that the identity of the conductive additive does not affect flash H_2 efficiency or yields. Small amounts of CO and CO_2 are produced when the conductive additive has atomic O content. Metcoke can be repeatedly used as a

conductive additive through simple sieve separation, further lowering costs associated with the conductive additive, with 92% of the metcoke recovered after 5 use cycles. The metcoke is converted to graphene after the first cycle but remains in large particles thus facilitating separation. Further, after the first cycle, no CO or CO_2 is produced since the O content has been removed (Figure 4d). Graphene quality is largely unaffected by both polymer and conductive additive type (Figure 4e,f).

Computational and experimental mechanistic study

Since no catalyst is present during the rapid FJH, the generation of flash H_2 likely proceeds through bond homolysis which deconstructs the polymer chains into the observed volatiles (Figure S7). The ultrafast heating rates and high temperatures (Figure 2b) allow for more complete deconstruction into the most thermodynamically favored products (Figure S8). The reaction mechanism for the FJH or laser vaporization-assisted transformation of amorphous or olefinic carbon into graphene has been previously attributed to mobile carbon nucleating the sheets through a seed-growth mechanism, which can achieve diffusion-controlled reaction kinetics at sufficiently high energy density.(*29*, *36–38*)

The growth of semicrystalline turbostratically stacked sheet-like graphene domains from small, wrinkled, and defective regions can be observed morphologically by SEM imaging as the sample resistance decreases (Figure 5a). Large areas of sheet-like morphologies are not observed until reaching temperatures >2,300 K, corresponding to an atomic C vapor pressure of ~10^{-4} Pa. This low vapor pressure, maintained for only milliseconds, is unlikely to allow for micron scale crystal growth, indicating another intermediate is required for the mobile carbon hypothesis.(*39*) The FJH process forms 1,3-butadiene, ethylene, and benzene as detected by GC-MS, which can

combine through aromatic polymerization, forming graphitic domains (Figure S9). Aromatic products are detected, with the overall amount and size of aromatics increasing as resistance is lowered and higher temperatures are achieved (Figure 5b). Polymerization of polyaromatic hydrocarbons has been previously demonstrated under high energy density conditions, such as in stars or under laser irradiation.(*40*, *41*) The detected polyaromatic hydrocarbons formed during FJH can be considered the seeds of eventual turbostratic graphene sheets, which grow through aromatic coupling of other mobile carbon species.

These findings are also studied computationally through molecular dynamics (MD) simulations with AIREBO interatomic potentials.(*42*, *43*) Following the structural characteristics of the HDPE, the system of long, highly intertwined PE strands was constructed.(*44*) Due to the high flexibility of the polymer chains at temperatures observed during FJH, smaller structures or those containing shorter chains displayed rapid unraveling mandating the use of chains with at least 150 carbon atoms.(*45*) The HDPE structure was generated through the iterative addition of carbon strands composed of a series of randomly oriented straight and curved segments, ensuring a significantly interwoven configuration (Figure 5c-d). Following experimental results, we compared the system behavior at 1500 K and 3000 K, representing samples with high (225 Ohm) and lower (30 Ohm) resistance, respectively. In both cases, the evolution of H_2 was observed throughout the simulation, with H_2 production significantly increased at higher temperatures (Figure 5e). The synthesis of short-chain hydrocarbons was also observed. The dehydrogenated and partially dehydrogenated carbon chains were observed to form bonds producing interconnected carbon networks and aromatic segments (Figure 5f), further proceeding to the formation of graphitic domains.

Life-cycle assessment and technoeconomic analysis

Life-cycle assessment (LCA) is a technique used to analyze the holistic environmental impacts and resource demands associated with production methods, allowing for direct comparisons.(*46*, *47*) The LCA conducted here compares the cradle-to-gate inputs, outputs, and demands associated with producing a functional unit of 1 kg of purified H_2 by various methods. LCA for the conversion of polyethylene into flash H_2 by the FJH process and a recently reported catalytic microwave-irradiation polymer deconstruction process are compared to the LCAs of other common H_2 production methods. Techno-economic analysis (TEA) similarly considers the associated costs, and thus estimates and compares economic feasibility of processes. Further details regarding the FJH and microwave deconstruction LCAs and TEAs can be found in the *Methods* in the *Supplemental Information,* Figure S10-S11, and Table S1-S3.

The flash H_2 process provides improvements in both cumulative energy demand (33-95% less energy) and greenhouse gas emissions (65-89% less emissions) when compared to other waste plastic or biomass deconstruction methods for H_2 production (Figure 5 g-h). Despite the FeAlOx/microwave deconstruction producing less than stoichiometric CO_2 for polyolefins, the process still produces significant emissions with a full weight equivalent of metal complex. Flash H_2 production compares favorably to current industrial methods, producing 84% less greenhouse gas emissions than steam methane reforming, while using 4% less energy than green H_2.

Since valuable turbostratic graphene is produced as a by-product of the FJH method, this provides a secondary value stream to improve economic competitiveness of flash H_2 production. For the purposes of this TEA, sale of this graphene is assumed at $3 per kg, similar to the current cost of some commodity plastics and only 5% of current market value of graphene (US$60 per kg) to present a “worst-case” scenario. Preliminary estimated cost for the flash H_2 with graphene sale

demonstrates that production costs are negative, -$4.24 per kg H_2, even at this unrealistically low sale price of graphene (Figure 5i). The $FeAlO_x$ catalyzed microwave deconstruction, despite producing high-value multiwalled carbon nanotubes with a higher simulated sale price of $16 per kg, still exhibits high production costs due to the energy-intensive microwave use and large amount of metal required. Flash H_2 presents a new leading technology for H_2 production (Figure 5j). Our findings demonstrate that FJH can be leveraged to produce negative-cost clean H_2 from waste materials. Increased understanding of the FJH mechanism and improvements in scalability will optimize the flash H_2 production efficiency.

Experimental details including equipment, materials, and methods are included in the SI.

References and Notes

1. A. Ajanovic, M. Sayer, R. Haas, The economics and the environmental benignity of different colors of hydrogen. *Int. J. Hydrog. Energy*. 47, 24136–24154 (2022).
2. S. van Renssen, The hydrogen solution? *Nat. Clim. Change*. 10, 799–801 (2020).
3. S. A. Grigoriev, V. N. Fateev, D. G. Bessarabov, P. Millet, Current status, research trends, and challenges in water electrolysis science and technology. *Int. J. Hydrog. Energy*. 45, 26036–26058 (2020).
4. S. Shiva Kumar, H. Lim, An overview of water electrolysis technologies for green hydrogen production. *Energy Rep.* 8, 13793–13813 (2022).
5. Z. J. Baum, L. L. Diaz, T. Konovalova, Q. A. Zhou, Materials Research Directions Toward a Green Hydrogen Economy: A Review. *ACS Omega*. 7, 32908–32935 (2022).

6. R. R. Beswick, A. M. Oliveira, Y. Yan, Does the Green Hydrogen Economy Have a Water Problem? *ACS Energy Lett.* 6, 3167–3169 (2021).

7. M. Hermesmann, T. E. Müller, Green, Turquoise, Blue, or Grey? Environmentally friendly Hydrogen Production in Transforming Energy Systems. *Prog. Energy Combust. Sci.* 90, 100996 (2022).

8. R. W. Howarth, M. Z. Jacobson, How green is blue hydrogen? *Energy Sci. Eng.* 9, 1676–1687 (2021).

9. N. Sazali, Emerging technologies by hydrogen: A review. *Int. J. Hydrog. Energy*. 45, 18753–18771 (2020).

10. Hydrogen Shot. *Energy.gov*, (available at https://www.energy.gov/eere/fuelcells/hydrogen-shot).

11. J. M. Garcia, M. L. Robertson, The future of plastics recycling. *Science*. 358, 870–872 (2017).

12. K. Lan, Y. Yao, Feasibility of gasifying mixed plastic waste for hydrogen production and carbon capture and storage. *Commun. Earth Environ.* 3, 1–11 (2022).

13. N. Cai, X. Li, S. Xia, L. Sun, J. Hu, P. Bartocci, F. Fantozzi, P. T. Williams, H. Yang, H. Chen, Pyrolysis-catalysis of different waste plastics over Fe/Al2O3 catalyst: High-value hydrogen, liquid fuels, carbon nanotubes and possible reaction mechanisms. *Energy Convers. Manag.* 229, 113794 (2021).

14. X. Jie, W. Li, D. Slocombe, Y. Gao, I. Banerjee, S. Gonzalez-Cortes, B. Yao, H. AlMegren, S. Alshihri, J. Dilworth, J. Thomas, T. Xiao, P. Edwards, Microwave-initiated catalytic

deconstruction of plastic waste into hydrogen and high-value carbons. *Nat. Catal.* 3, 902–912 (2020).

15. D. X. Luong, K. V. Bets, W. A. Algozeeb, M. G. Stanford, C. Kittrell, W. Chen, R. V. Salvatierra, M. Ren, E. A. McHugh, P. A. Advincula, Z. Wang, M. Bhatt, H. Guo, V. Mancevski, R. Shahsavari, B. I. Yakobson, J. M. Tour, Gram-scale bottom-up flash graphene synthesis. *Nature*. 577, 647–651 (2020).

16. W. Chen, J. T. Li, Z. Wang, W. A. Algozeeb, D. X. Luong, C. Kittrell, E. A. McHugh, P. A. Advincula, K. M. Wyss, J. L. Beckham, M. G. Stanford, B. Jiang, J. M. Tour, Ultrafast and Controllable Phase Evolution by Flash Joule Heating. *ACS Nano*. 15, 11158–11167 (2021).

17. W. A. Algozeeb, P. E. Savas, D. X. Luong, W. Chen, C. Kittrell, M. Bhat, R. Shahsavari, J. M. Tour, Flash Graphene from Plastic Waste. *ACS Nano*. 14, 15595–15604 (2020).

18. K. M. Wyss, R. D. De Kleine, R. L. Couvreur, A. Kiziltas, D. F. Mielewski, J. M. Tour, Upcycling end-of-life vehicle waste plastic into flash graphene. *Commun. Eng.* 1, 1–12 (2022).

19. K. M. Wyss, W. Chen, J. L. Beckham, P. E. Savas, J. M. Tour, Holey and Wrinkled Flash Graphene from Mixed Plastic Waste. *ACS Nano* (2022), doi:10.1021/acsnano.2c00379.

20. K. M. Wyss, B. Deng, J. M. Tour, Upcycling and urban mining for nanomaterial synthesis. *Nano Today*. 49, 101781 (2023).

21. S. K. Tiwari, S. Sahoo, N. Wang, A. Huczko, Graphene research and their outputs: Status and prospect. *J. Sci. Adv. Mater. Devices*. 5, 10–29 (2020).

22. M. J. Allen, V. C. Tung, R. B. Kaner, Honeycomb Carbon: A Review of Graphene. *Chem. Rev.* 110, 132–145 (2010).

23. K. M. Wyss, D. X. Luong, J. M. Tour, Large-Scale Syntheses of 2D Materials: Flash Joule Heating and Other Methods. *Adv. Mater.* 34, 2106970 (2022).

24. O. Li, S. Tamrakar, Z. Iyigundogdu, D. Mielewski, K. Wyss, J. M. Tour, A. Kiziltas, Flexible polyurethane foams reinforced with graphene and boron nitride nanofillers. *Polym. Compos.* n/a, doi:10.1002/pc.27183.

25. P. A. Advincula, V. Granja, K. M. Wyss, W. A. Algozeeb, W. Chen, J. L. Beckham, D. X. Luong, C. F. Higgs, J. M. Tour, Waste plastic- and coke-derived flash graphene as lubricant additives. *Carbon*. 203, 876–885 (2023).

26. A. P. Kauling, A. T. Seefeldt, D. P. Pisoni, R. C. Pradeep, R. Bentini, R. V. B. Oliveira, K. S. Novoselov, A. H. C. Neto, The Worldwide Graphene Flake Production. *Adv. Mater.* 30, 1803784 (2018).

27. C. Backes, A. M. Abdelkader, C. Alonso, A. Andrieux-Ledier, R. Arenal, J. Azpeitia, N. Balakrishnan, L. Banszerus, J. Barjon, R. Bartali, S. Bellani, C. Berger, R. Berger, M. M. B. Ortega, C. Bernard, P. H. Beton, A. Beyer, A. Bianco, P. Bøggild, F. Bonaccorso, G. B. Barin, C. Botas, R. A. Bueno, D. Carriazo, A. Castellanos-Gomez, M. Christian, A. Ciesielski, T. Ciuk, M. T. Cole, J. Coleman, C. Coletti, L. Crema, H. Cun, D. Dasler, D. D. Fazio, N. Díez, S. Drieschner, G. S. Duesberg, R. Fasel, X. Feng, A. Fina, S. Forti, C. Galiotis, G. Garberoglio, J. M. García, J. A. Garrido, M. Gibertini, A. Gölzhäuser, J. Gómez, T. Greber, F. Hauke, A. Hemmi, I. Hernandez-Rodriguez, A. Hirsch, S. A. Hodge, Y. Huttel, P. U. Jepsen, I. Jimenez, U. Kaiser, T. Kaplas, H. Kim, A. Kis, K. Papagelis, K. Kostarelos, A. Krajewska, K. Lee, C. Li, H. Lipsanen, A. Liscio, M. R. Lohe, A. Loiseau,

L. Lombardi, M. F. López, O. Martin, C. Martín, L. Martínez, J. A. Martin-Gago, J. I. Martínez, N. Marzari, Á. Mayoral, J. McManus, M. Melucci, J. Méndez, C. Merino, P. Merino, A. P. Meyer, E. Miniussi, V. Miseikis, N. Mishra, V. Morandi, C. Munuera, R. Muñoz, H. Nolan, L. Ortolani, A. K. Ott, I. Palacio, V. Palermo, J. Parthenios, I. Pasternak, A. Patane, M. Prato, H. Prevost, V. Prudkovskiy, N. Pugno, T. Rojo, A. Rossi, P. Ruffieux, P. Samorì, L. Schué, E. Setijadi, T. Seyller, G. Speranza, C. Stampfer, I. Stenger, W. Strupinski, Y. Svirko, S. Taioli, K. B. K. Teo, M. Testi, F. Tomarchio, M. Tortello, E. Treossi, A. Turchanin, E. Vazquez, E. Villaro, P. R. Whelan, Z. Xia, R. Yakimova, S. Yang, G. R. Yazdi, C. Yim, D. Yoon, X. Zhang, X. Zhuang, L. Colombo, A. C. Ferrari, M. Garcia-Hernandez, Production and processing of graphene and related materials. *2D Mater.* 7, 022001 (2020).

28. A. C. Ferrari, D. M. Basko, Raman spectroscopy as a versatile tool for studying the properties of graphene. *Nat. Nanotechnol.* 8, 235–246 (2013).

29. K. M. Wyss, J. T. Li, P. A. Advincula, K. V. Bets, W. Chen, L. Eddy, K. J. Silva, J. L. Beckham, J. Chen, W. Meng, B. Deng, S. Nagarajaiah, B. I. Yakobson, J. M. Tour, Upcycling of Waste Plastic into Hybrid Carbon Nanomaterials. *Adv. Mater.* (2023).

30. S. Shallcross, S. Sharma, E. Kandelaki, O. A. Pankratov, Electronic structure of turbostratic graphene. *Phys. Rev. B*. 81, 165105 (2010).

31. Y. Cao, V. Fatemi, S. Fang, K. Watanabe, T. Taniguchi, E. Kaxiras, P. Jarillo-Herrero, Unconventional superconductivity in magic-angle graphene superlattices. *Nature*. 556, 43–50 (2018).

32. K. M. Wyss, Z. Wang, L. B. Alemany, C. Kittrell, J. M. Tour, Bulk Production of Any Ratio 12C:13C Turbostratic Flash Graphene and Its Unusual Spectroscopic Characteristics. *ACS Nano*. 15, 10542–10552 (2021).

33. K. M. Wyss, J. L. Beckham, W. Chen, D. X. Luong, P. Hundi, S. Raghuraman, R. Shahsavari, J. M. Tour, Converting plastic waste pyrolysis ash into flash graphene. *Carbon*. 174, 430–438 (2021).

34. Universal Matter Material Science: Graphene In A Flash. *Univers. Matter*, (available at https://www.universalmatter.com/).

35. J. C. Petersen, "Chapter 14 Chemical Composition of Asphalt as Related to Asphalt Durability" in *Developments in Petroleum Science*, T. F. Yen, G. V. Chilingarian, Eds. (Elsevier, 2000; https://www.sciencedirect.com/science/article/pii/S0376736109702857), vol. 40 of *Asphaltenes and Asphalts, 2*, pp. 363–399.

36. M. G. Stanford, K. V. Bets, D. X. Luong, P. A. Advincula, W. Chen, J. T. Li, Z. Wang, E. A. McHugh, W. A. Algozeeb, B. I. Yakobson, J. M. Tour, Flash Graphene Morphologies. *ACS Nano* (2020), doi:10.1021/acsnano.0c05900.

37. J. L. Beckham, K. M. Wyss, Y. Xie, E. A. McHugh, J. T. Li, P. A. Advincula, W. Chen, J. Lin, J. M. Tour, Machine Learning Guided Synthesis of Flash Graphene. *Adv. Mater.* 34, 2106506 (2022).

38. F. Kokai, M. Ishihara, A. Koshio, A. Nakayama, Y. Koga, Fabrication of some graphitic polyhedra and balloon-like particles. *Diam. Relat. Mater.* 16, 1264–1268 (2007).

39. L. C. Lopes, L. C. da Silva, B. G. Vaz, A. R. M. Oliveira, M. M. Oliveira, M. L. M. Rocco, E. S. Orth, A. J. G. Zarbin, Facile room temperature synthesis of large graphene sheets from simple molecules. *Chem. Sci.* 9, 7297–7303 (2018).

40. I. J. Webster, J. L. Beckham, N. D. Johnson, M. A. Duncan, Photochemical Synthesis and Spectroscopy of Covalent PAH Dimers. *J. Phys. Chem. A*. 126, 1144–1157 (2022).

41. C. S. Contreras, F. Salama, LABORATORY INVESTIGATIONS OF POLYCYCLIC AROMATIC HYDROCARBON FORMATION AND DESTRUCTION IN THE CIRCUMSTELLAR OUTFLOWS OF CARBON STARS. *Astrophys. J. Suppl. Ser.* 208, 6 (2013).

42. S. J. Stuart, A. B. Tutein, J. A. Harrison, A reactive potential for hydrocarbons with intermolecular interactions. *J. Chem. Phys.* 112, 6472–6486 (2000).

43. D. W. Brenner, O. A. Shenderova, J. A. Harrison, S. J. Stuart, B. Ni, S. B. Sinnott, A second-generation reactive empirical bond order (REBO) potential energy expression for hydrocarbons. *J. Phys. Condens. Matter*. 14, 783 (2002).

44. M. S. Miao, M.-L. Zhang, V. E. Van Doren, C. Van Alsenoy, J. L. Martins, Density functional calculations on the structure of crystalline polyethylene under high pressures. *J. Chem. Phys.* 115, 11317–11324 (2001).

45. K. V. Bets, B. I. Yakobson, Spontaneous twist and intrinsic instabilities of pristine graphene nanoribbons. *Nano Res.* 2, 161–166 (2009).

46. S. Hellweg, L. Milà i Canals, Emerging approaches, challenges and opportunities in life cycle assessment. *Science*. 344, 1109–1113 (2014).

47. Y. Khojasteh Salkuyeh, B. A. Saville, H. L. MacLean, Techno-economic analysis and life cycle assessment of hydrogen production from natural gas using current and emerging technologies. *Int. J. Hydrog. Energy*. 42, 18894–18909 (2017).

Acknowledgements and Funding Statement

JMT and BYI thank the US Army Corps of Engineers, ERDC, for their support (W912HZ-21-2-0050). JMT also thanks the Air Force Office of Scientific Research (FA9550-22-1-0526). KMW and JLB thank the National Science Foundation for Graduate Research Fellowship Program funding. KVB and BIY additionally thank the Office of Naval Research (N00014-22-1-2788). We acknowledge the Rice Electron Microscope Center (EMC) for consultation and instrument maintenance.

Competing interests: Rice University owns the intellectual property (IP) on the process to generate flash H_2 from plastic waste, and that IP is currently unlicensed. Universal Matter Inc. has licensed IP from Rice University on the synthesis of flash graphene from carbon sources. JMT is a stockholder in that company, but not an officer, director, or employee. Conflicts of interest are mitigated through compliance and reporting with the Rice University Office of Sponsored Programs and Research Compliance.

Data and materials availability: The data supporting the findings of this study are available within the article and its Supplementary Information. The source data generated in this study have been deposited in the Zenodo database. Other relevant data are available from the corresponding authors upon request. Source data are provided with this paper.

Supplementary Materials

Equipment details

Materials and Methods

Fig. S1 to S11

Tables S1 to S3

References S1 to S11

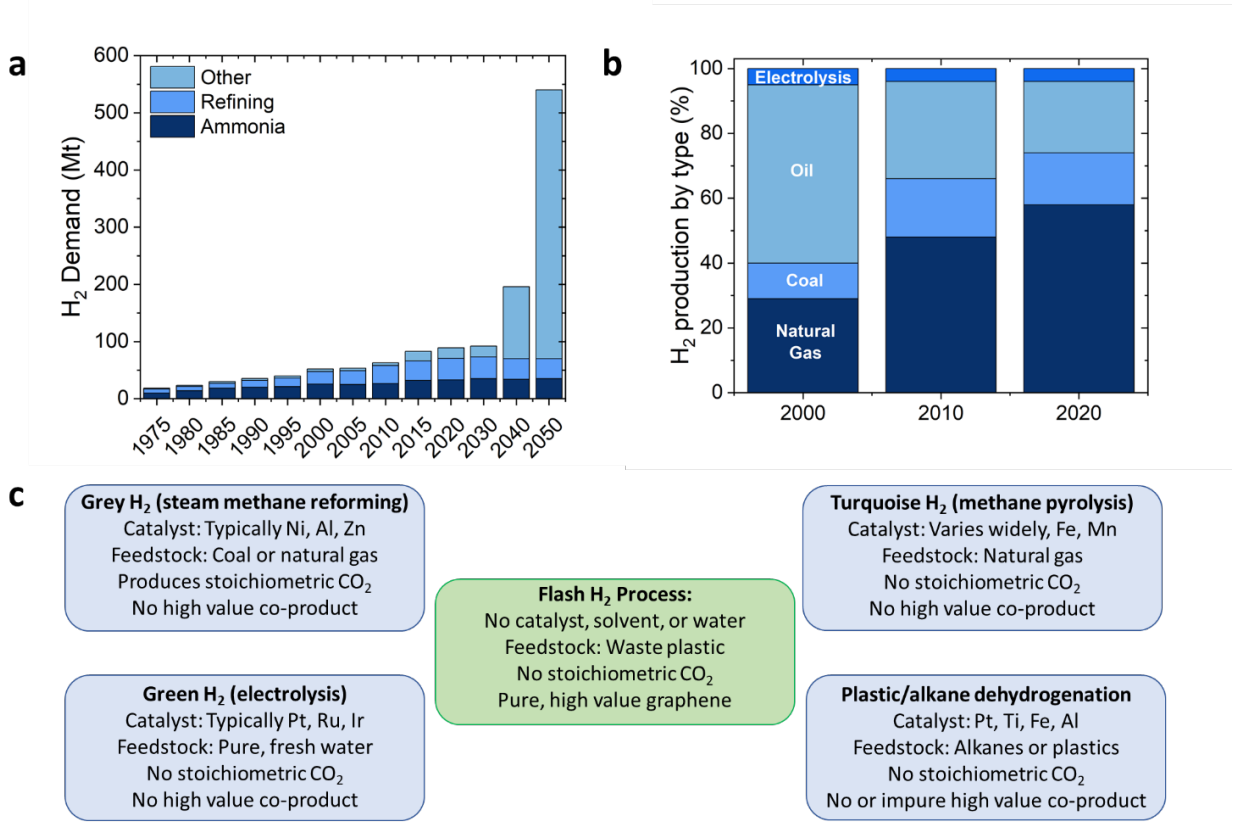

Fig. 1: Current state of H_2 production and projected demand. a, Historic and projected demand for H_2, separated by use. **b,** The source of hydrogen historically produced, separated by feedstock. **c,** A scheme comparing the other H_2 production methods with the flash H_2 process presented here.

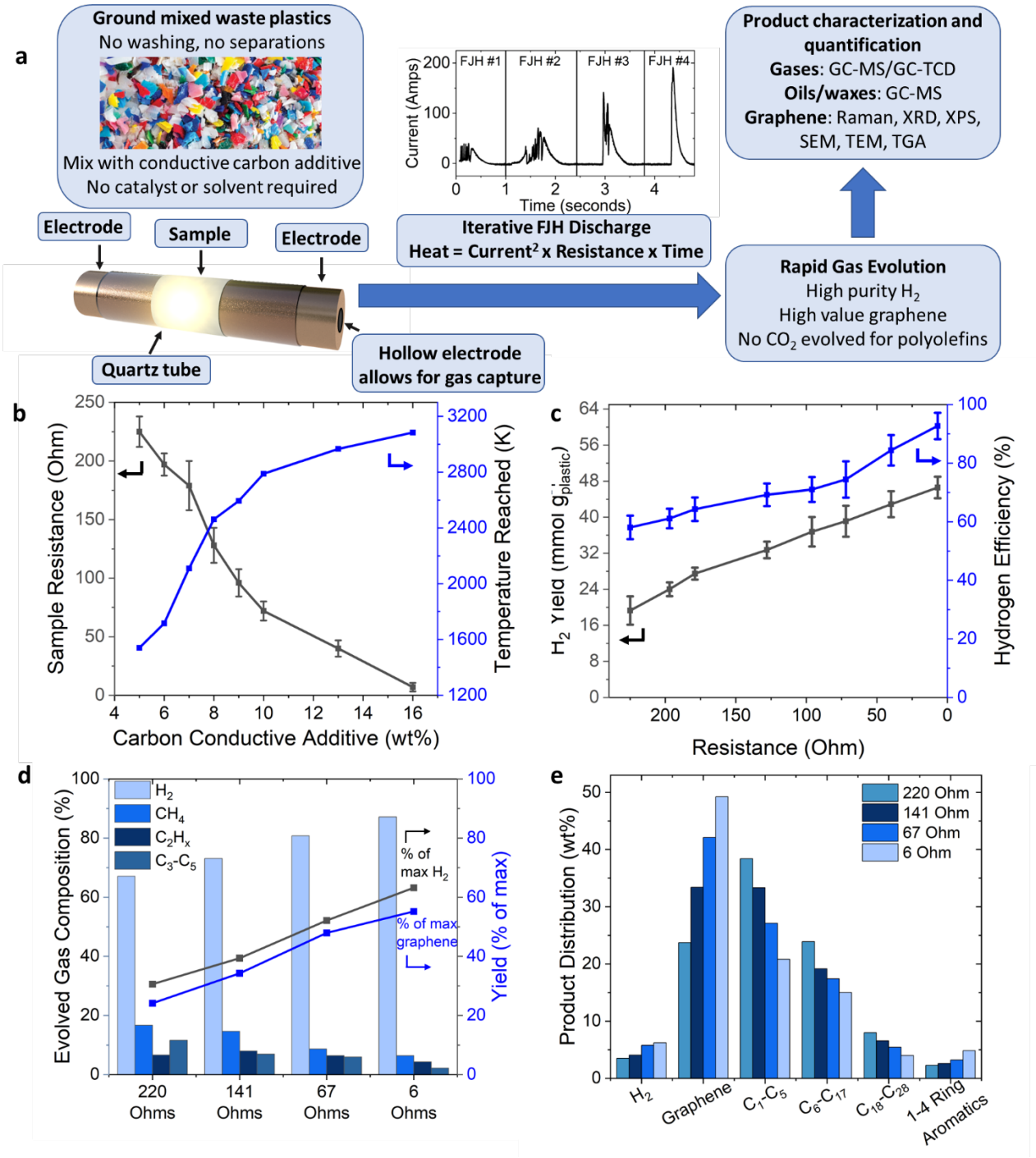

Fig. 2 Catalyst-free deconstruction of polyethylene to yield flash H_2 and graphene. a, A schematic showing the typical flash Joule heating process used to convert waste plastic into flash H_2, with the inset graph showing the current discharge as a function of time over four iterative FJH treatments at 6 Ohm initial resistance sample to deconstruct the waste plastic. **b,** The resistance of

plastic sample before treatment (black trace) and peak temperature reached during FJH treatment (red trace) as a function of conductive carbon black mixed with waste polyethylene. Error bars represent the standard deviation, N=3. **c,** The relationship between initial sample resistance, H_2 yield (black trace), and hydrogen efficiency (red trace) in the FJH deconstruction of polyethylene. Hydrogen efficiency is the total mass of atomic hydrogen contained in all gas phase products, as compared to the atomic hydrogen content of the starting polymer. Error bars represent the standard deviation, N=3. **d,** The relationship between initial sample resistance and the gaseous products and yield of H_2 and graphene resulting from polyethylene deconstruction, where the bar graph corresponds to partial pressure of gas, while the line graph corresponds to the yield of H_2 (black trace) or graphene (blue trace) compared to the amount of atomic H and C present in the starting mixture. **e,** Mass balance of polyethylene deconstruction as resistance varies.

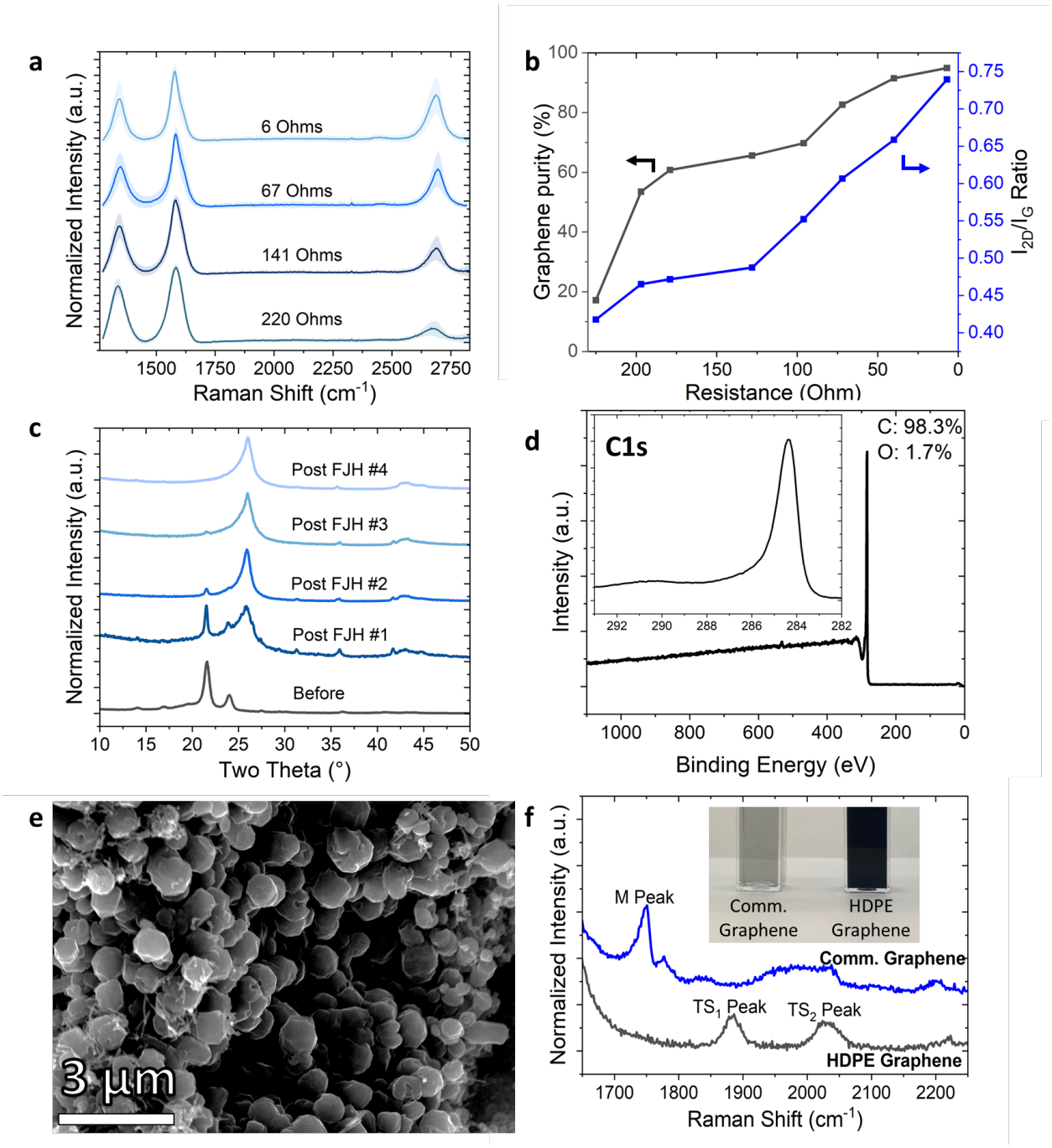

Fig. 3: Characterization of polyethylene derived graphene. a, The average Raman spectra (100 unique spectra, over a 1 mm^2 area) of graphene produced as initial polyethylene sample resistance is varied. The standard deviation is represented by the shaded area. **b,** Raman spectroscopy determined graphene purity and I_{2D}/I_G ratio as a function of sample resistance, showing the average of 100 unique spectra per sample. **c,** Bulk powder X-Ray diffraction analysis of solid produced

from a 6 Ohm sample of polyethylene over iterative FJH treatment, as compared to the initial feedstock mixture, showing bulk conversion of polyethylene into pure graphene. **d,** X-ray photoelectron spectroscopy analysis of a 6 Ohm sample produced graphene, with inset high-resolution analysis of the C1s transition. **e,** Scanning electron micrograph of crystalline graphene produced from a 6 Ohm sample of polyethylene. **f,** High resolution Raman spectra demonstrating the presence of the TS_1 and TS_2 peaks in FJH graphene samples indicating turbostratic stacking, while the presence of the M peak in commercial graphene samples indicating AB stacking. An inset photograph shows polyethylene-derived graphene and commercial graphene dispersed in water-Pluronic (F-127) solution (1 wt%) by sonication and centrifuged, showing turbostratic stacking significantly improves graphene dispersibility.

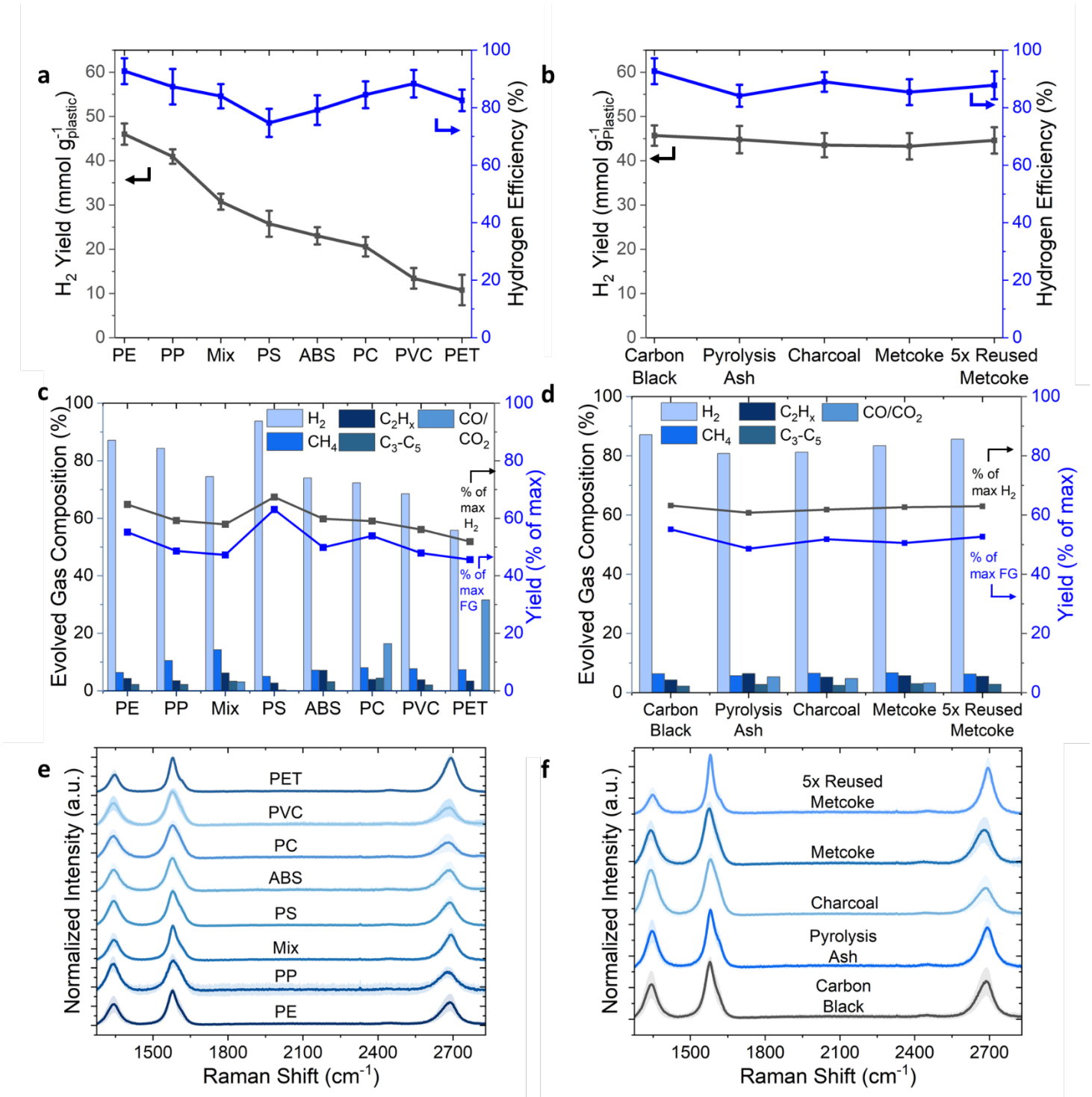

Fig. 4: Process generality for other waste polymers, mixtures, and low-cost conductive additives. a, Flash H_2 yield (black) and efficiency (blue) as waste plastic type varies. Error bars represent the standard deviation, N=3. **b,** Flash H_2 yield (black) and efficiency (blue) as conductive

additive varies. Error bars represent the standard deviation, N=3. **c,d,** Gaseous products evolved, with flash H_2 and graphene yields calculated, as (c) waste plastic type or (d) conductive additives are varied. The bar graph corresponds to partial pressure of gas, while the line graph corresponds to the yield of flash H_2 (black) or graphene (blue) compared to the amount of atomic H and C present in the starting mixture. **e-f,** Average Raman spectra (100 unique spectra, over a 1 mm^2 area) as (e) waste plastic type or (f) conductive additive varies. The shaded area represents the standard deviation in spectra. The 'Mix' contains 20% low-density polyethylene (LDPE), 20% high-density polyethylene (HDPE), 15% polystyrene (PS), 10% polyvinylchloride (PVC), and 15% polyethylene terephthalate (PET). Other polymers tested include acrylonitrile-butadiene-styrene (ABS) and polycarbonate (PC).

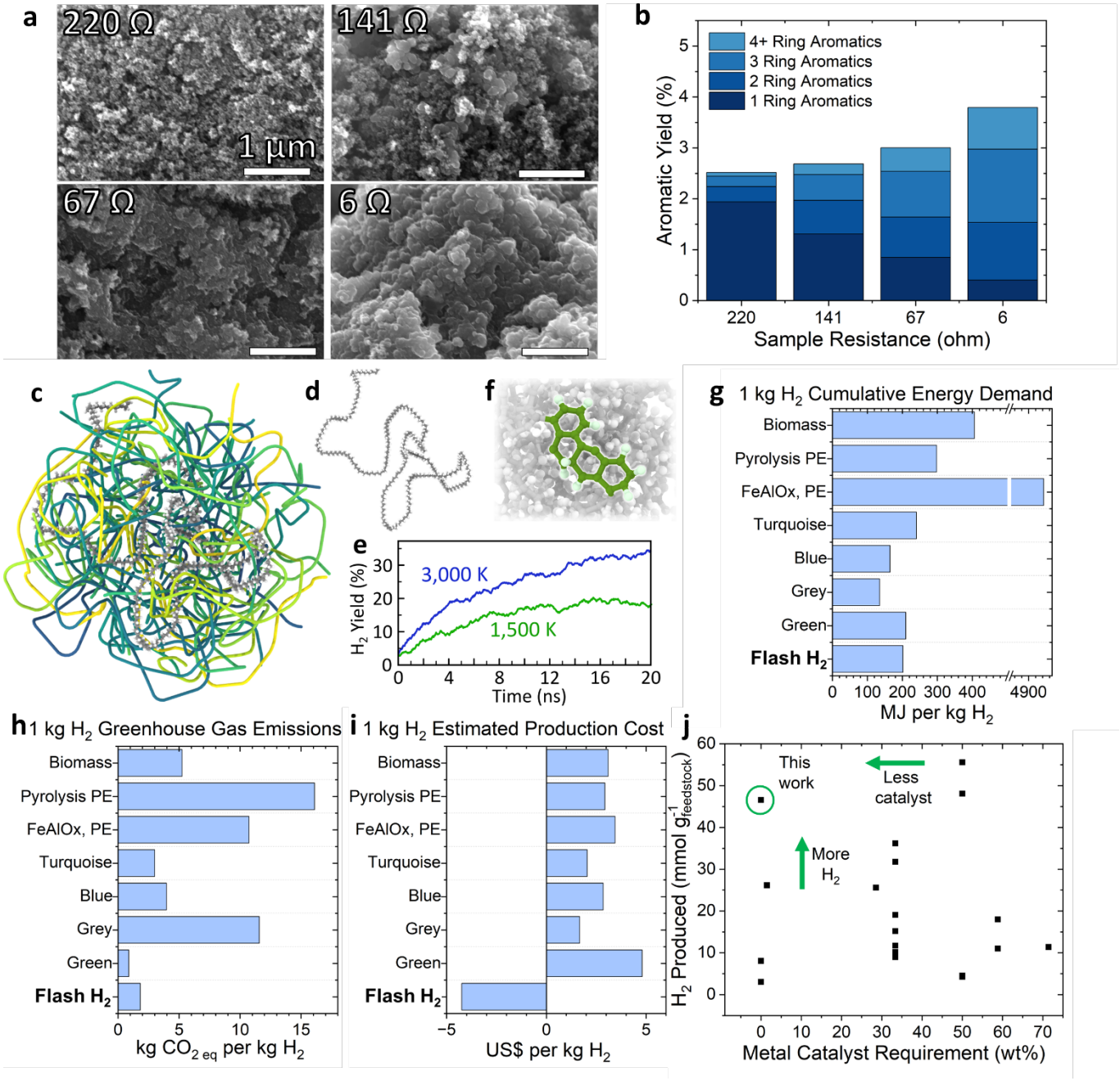

Fig. 5: Mechanistic assessment of the catalyst free FJH deconstruction process, and comparison to current industrial and laboratory methods. a, SEM micrographs examining the graphene morphology resulting from the deconstruction of HDPE as a function of initial resistance. All scale bars are the same. **b,** Aromatic products evolved, as a function of sample resistance, showing that aromatic formation and polymerization occurs more readily at lower sample

resistances. **c-f,** Atomistic simulations of the FJH reaction including (c) a simplified representation of the atomistic model of a HDPE particle showing predominantly carbon spines of polymers where colors indicate individual polymer strands, d) an individual polymer strand in full atomistic details as extracted from c, e) H_2 production during the simulation at 1,500 K and 3,000 K, and f) formation of aromatic networks at the early stages of HDPE deconstruction. **g-i,** The (g) cumulative energy demand, (h) greenhouse gas emissions, and (i) estimated production cost resulting from the production of 1 kg H_2 using different methods. FJH PE is the flash Joule heating method to flash H_2 disclosed here. The data and source for each data point is available in Table S1a. Key assumptions used here include that the power source for all is green energy, thus no emissions are contributed from powering each method. The $FeAlO_x$ PE process involves microwave irradiation. The estimated production cost of the FJH PE and $FeAlO_x$ PE processes include the sale of high-value carbon coproducts. The estimated cost of the graphene is <5% the current cost of bulk graphene. **j,** Comparing different methods that produce H_2 from waste plastic, biomass, or hydrocarbons. The data and source for each data point is available in Table S1b.

Supplementary Materials for

Synthesis of clean hydrogen gas from waste plastic at zero net cost

Kevin M. Wyss[1], Karla J. Silva[1], Ksenia V Bets[2], Wala A. Algozeeb[1], Carter Kittrell[1], Carolyn H. Teng[1], ChiHun Choi[1], Weiyin Chen[1], Jacob Beckham[1], Boris I. Yakobson,[1,2,3,*] and James M. Tour[1,2,3,*]

Corresponding author: biy@rice.edu; tour@rice.edu

The PDF file includes:

Equipment:

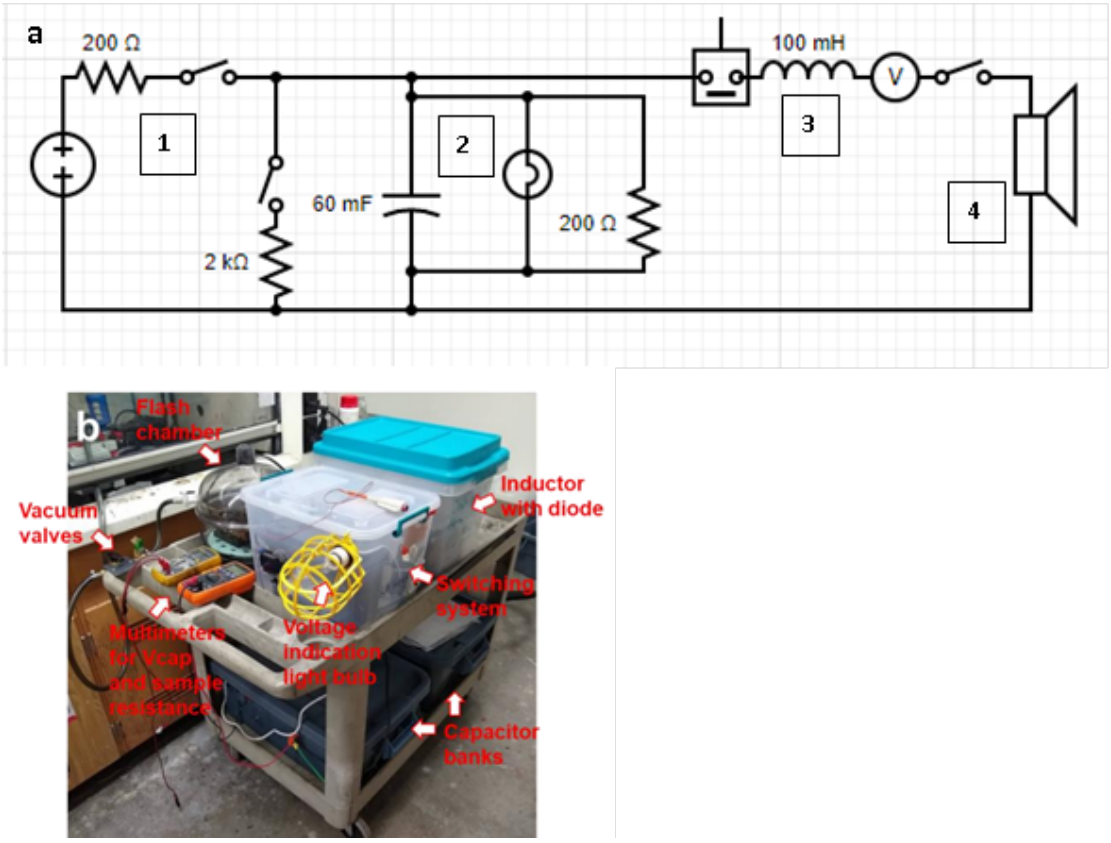

Figure S1. a) Simple circuit schematic of FJH equipment; b) picture of FJH station, as published in previous work.(*1–3*) For FJH specifications and safety notes, see our prior work.(*1*)

Brief overview of components shown in Figure S1a:

1) DC voltage source provided by normal AC wall outlet, rectified through AC-DC converter.
2) Capacitor bank, with indicator light, an incandescent bulb safety feature that turns on when capacitors charged.
3) Computer controlled IGBT for current discharge control, followed by inductor, followed by Hall effect sensor. Computer controlled *via* custom programmed LabView software platform.
4) Sample holder in desiccator under gentle vacuum to facilitate outgassing of sublimed heteroatoms.

CAUTION: There is a risk of electrical shock or even electrocution so the safety features previously discussed[1] should be implemented. The following list[1] is not intended to be comprehensive but demonstrative of the protocols needed to minimize risk.

1. Enclose or carefully insulate all wire connections.

2. All connections, wires and components must be suitable for the high voltages and currents.

3. Be aware that component failure could cause high voltage to appear in unexpected places, such as heat sinks on the switching transistors.

4. Control wires should have opto-isolators rated for high voltage.

5. Provide a visible charge indicator. A 230 V clear glass incandescent light bulb is a good choice as the glow on the filament also provides an approximate indicator of the amount of charge on the capacitor bank. Bright light = danger!

6. Do not use toggle switches with metal toggles. If an arc develops, the metal toggle could become charged.

7. One hand rule. Use only one hand when working on the system, with the other hand not touching any grounded surface.

8. Install bleed resistors in the range of 100,000 Ohm on each capacitor so that charge will always bleed off in ~1 h.

9. Provide a mechanical discharge circuit breaker switch connected to a power resistor of a few hundred ohms to rapidly bleed off the capacitor charge.

10. Provide a "kill" circuit breaker switch to disconnect the sample holder from the capacitor bank.

11. Provide an AC disconnect circuit breaker switch.

12. Post high voltage warning signs on the apparatus.

13. Use of circuit breakers as switches. Circuit breakers have built-in arc suppression that can interrupt 1000 amps or more. Conventional switches do not have such a high level of arc suppression and can burn out or weld closed due to the high current pulses.

14. Use circuit breakers rated for DC voltage. Most AC circuit breakers have a DC rating ½ the voltage or less, since DC arcs are much more difficult to suppress. Circuit breakers designed for DC solar power systems are a good choice.

15. When choosing circuit breakers, choose by the time curves typical for 0.1 s, rather than the steady state current rating. K-type DC circuit breakers will have ~10x higher trip current at 0.1 s compared to their rated current, and Z-type breakers will have ~4x higher trip current at 0.1 s. This "delayed trip" designed into most circuit breakers will allow much higher pulse currents than the steady state rating of the breaker.

16. Include a small amount of inductance in the discharge circuit to limit the rise time to a millisecond or more. Extremely fast discharges can damage components and cause RF interference with other lab apparatii.

17. Keep in mind that the system can discharge many thousands of Joules in milliseconds, which can cause components such as relays or even capacitors to explode. These components should be enclosed to protect against both high voltage and possible flying debris.

18. Keep a voltmeter with high voltage test leads handy at all times. When working on the capacitor bank, always check the voltage on each. A broken wire or loose connection could leave the capacitor in a charged state.

19. Wear thick rubber gloves when using the apparatus to protect from electrocution.

20. All users should be properly trained by an experienced electrical technician.

21. Welder's glasses should be worn to minimize eye damage risk by the bright emitted light resulting from the flash (IR and visible photons can cause eye damage).

Materials:

Amorphous CB Pearls BP-2000 (Cabot), metallurgical coke (SunCoke), charcoal (EnviroSupply & Service), and waste plastic pyrolysis ash treated at 540°C (Shangqiu Zhongming Eco-Friendly Equipment Co., Ltd in Shangqiu City, Henan, China) were used as received. Plastic waste was collected from household waste, including carbonated beverage bottles (PET), milk jugs (HDPE), grocery bags (LDPE), food packaging (PS), coffee cups (PP), piping (PVC), CD cases (PC), and LEGO bricks (ABS). Plastic waste was ground using an electric hammer mill (CGoldenWall, Model DF-15) and was sieved to only use particles smaller than 1 mm (#18 sieve). Pluronic-F127, a non-ionic surfactant, was obtained from Millipore-Sigma. Commercial graphene samples (H25 grade, XGScience) were used without further purification. HPLC grade hexane, toluene, and acetone, used for rinsing the waxes and oils from the volatile gas trap were used as received. Standard gas mixtures used for calibration and quantification of reaction products, and high purity carrier gases, were obtained from AirGas. Standard hydrocarbon mixtures and polyaromatic hydrocarbon mixtures were used to characterize and quantify the oils and waxes produced.

Methods:

The reaction precursors include (1) the postconsumer plastic ground by hammer mill (CGoldenWall, Model DF-15) and filtered through a 1.5 mm sieve and used without the need for any rinsing or pretreatment, and (2) a small amount of conductive additive which may include

graphite, graphene, metcoke, carbon black, etc. As demonstrated in Figure 2b the amount of conductive additive (in that plot it is Carbon Black BP-2000, Cabot), determines the initial resistance of the sample which impacts the temperature of the FJH reaction. When other conductive additives, such as pyrolysis, metcoke, or charcoal are used, larger wt% of conductive additive may be required to reach an equivalent resistance. Similarly, if smaller grain size feedstocks such as asphaltene powders are used, then a larger amount of conductive additive must be used. The amount of additive required is determined by the particle size and conductivity of the additive as well as the feedstock. Once the reaction precursors are mixed thoroughly by mortar and pestle, the resulting in a black/gray powder mixture can undergo the flash Joule heating process. Flash Joule heating the mixture of precursors is shown in **Figure 2a**, the mixture (0.5 g total, 0.08 g conductive additive Carbon Black BP-2000 from Cabot and 0.42 g polymer) is loaded into a quartz tube and compressed to have a resistance of 5-10 Ohm. A pellet of copper wool is used as an electrode to allow for gas escape, and a graphite rod acts as the electrode on the other side. The metal electrodes have sealing o-rings to create a gas-tight seal. A hollow electrode is required to allow for the release and capture of volatiles in a Pyrex Schlenk flask that has been flushed with Ar and evacuated to -28 kPa of vacuum. The entire system is leak-tight, holding the vacuum for at least ~15 min after the valve to the vacuum is closed. Images of the system are shown below as reproduced from previous work.(*4*)

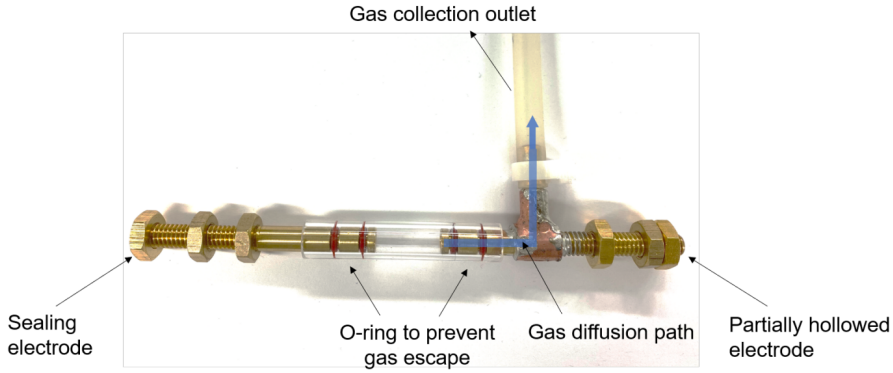

Figure S2. A picture of the system to collect the gases evolved by FJH.(*4*) The reaction feedstock is compressed between the two electrodes.

Then, flash Joule heating occurs, by charging a capacitor bank (220 mF) to 100-130 V. This is then discharged through the sample at very fast rates (typically less than 3 s) either using complete and non-modulated discharge. This process is repeated 3-4 times, until a singular sharp current discharge pulse is observed (inset in Figure 2a) and no more gas is evolved, as judged by a pressure gauge attached to the volatile trap. The interruptions in current discharge in the first 3 pulses are a result of volatiles leaving the system, temporarily increasing the resistance of the sample, thus lowering the amount of current able to pass through the sample. A pressure gauge attached to the volatile trap is used to measure the amount of volatiles evolved. Gas chromatography-thermal conductivity detector (GC-TCD) is then used to measure the partial pressure of H_2 in the mixture, which can then be used to determine the amount of H_2 evolved by the process using the ideal gas equation and the experimentally determined pressure, temperature, and volume of evolved gases. GC-TCD can also detect methane and CO, if present. Syringe headspace sampling of the volatile trap is also analyzed by GC-mass spectrometry (GC-MS), which detects and quantifies the small hydrocarbons produced (up to C_6 species) as well as CO_2

and water. The volatile trap can also be rinsed with a variety of solvents to study oil, wax, or aromatic species by injecting this rinse into the GC-MS. Standard analyte mixtures (of gases, oils, and aromatics) allow for the quantification of substances produced by the FJH deconstruction of plastics. The resulting graphene powder can be removed from the quartz tube, weighed, and characterized after grinding briefly by mortar and pestle and used without purification. The resulting hydrocarbon gas, oil, and wax minor byproducts expectedly vary with polymer identity, and some monomers, dimers, or oligomers of the parent polymers can be observed.

Characterization Methods:

Gaseous products were analyzed using an Agilent 8890 GC with 5977 B MSD and G4407 TCD. A carrier gas of Ar was used for the TCD to allow accurate H_2 detection, while a carrier gas of He was used for MSD analysis. The instrument is equipped with an Agilent HP-5ms low-bleed column (30 m, 0.25 mm internal diameter, 0.25 μm film). For permanent gas analysis, the instrument equipped with two Agilent 0.5 m HayeSep Q packed columns in series (Agilent part number G3591-82023), followed by an Agilent 2.44 m 5Å MolSieve column (Agilent part number G3591-81022), using a carrier gas of Ar. Quantification of compounds is conducted using high-purity standard gas or analyte mixtures, using peak integration to determine unknown concentration.

Raman spectra were collected using a Renishaw inVia Raman microscope outfitted with a 5 mW 532 nm laser. A 50x objective lens was used to collect all spectra. Analysis of Raman spectra, including peak intensity ratios, utilize the height of the peak. Custom Python scripts were used to analyze Raman spectral mapping data. Briefly, spectra were smoothed using a Savitsky-Golay filter, background-corrected using a polynomial fit, and averaged to give bulk sample characteristics. The LiveTrack software was automatically used to adjust focus between spectra.

If a G peak could not be identified within the collected spectrum, the spectrum was assumed to be poorly focused and was not employed in the analysis. This occurred <3% of the time. XPS data was collected using a PHI Quantera SXM Scanning X-Ray Microprobe with a base pressure of 5 × 10^{-9} Torr. Survey spectra were recorded using 0.5 eV step sizes with a pass energy of 140 eV. Elemental spectra were recorded using 0.1 eV step sizes with a pass energy of 26 eV. All the XPS spectra were corrected using the C1s peaks (284.6 eV) as reference. TGA thermograms were collected using a TA Instruments Q-600 Simultaneous TGA/DSC using alumina pans, with a heating rate of 5 °C min^{-1} up to 780 °C. Air atmosphere at a flow rate of 80 mL min^{-1} was used to purge the sample chamber. Powder XRD spectra were collected using a Rigaku SmartLab II using zero background sample holders at a scan rate of 1º min^{-1} and a 0.05º step size. SEM images were taken with a FEI Helios Nanolab 660 Dual Beam SEM System. A voltage of 15 keV was employed in imaging. TEM and SAED images were obtained on a JEOL 2100 field emission transmission electron microscope at an acceleration voltage of 200 kV. Samples were prepared by drop casting extremely dilute graphene/ethanol solutions on to lacey carbon grids.

Dispersibility Testing:

Graphene was dispersed in a 1% surfactant aqueous solution using Pluronic-F127, a non-ionic polyol surfactant. Varying amounts of ground graphene powder were weighed into centrifuge tubes, and solvent was added to yield the initial loading concentration (~1 mg graphene powder mL^{-1} of solvent). The centrifuge tubes were then sonicated in a cup-horn sonicator for 10 min (Cole-Parmer Qsonica 448) and centrifuged at 550 relative centrifugal force for 5 min to remove larger aggregates. The supernatant was decanted after centrifugation and diluted 100x since the graphene concentration leads to a very high absorbance. The absorbance of the solution was

measured at 660 nm. The concentration was determined using Beer's Law with an extinction coefficient of 66 L g^{-1} cm^{-1}.

Life-Cycle Assessment and Techno-economic Assessment

A cradle-to-gate ISO complaint life-cycle assessment consists of a systematic analysis of the demands and impacts associated with a product from raw materials required for synthesis to the processing and manufacturing of the product and does not examine the final disposal of reaction by-products or consider the end-use application or disposal of the product. The specific goal of this life-cycle assessment is to evaluate the demands and environmental impacts resulting from the FJH production of H_2 to compare with literature benchmarks studying the production of H_2 synthesized using other methods. The system considered here covers three main steps: raw material production, reaction feedstock preparation, and FJH or microwave reaction. Transportation of raw materials is not considered here, and a lab-scale process is assumed. The functional unit considered here is 1 kg of high purity H_2. The environmental impacts pertaining to the production of waste polyethylene were not considered in this study since it is a waste product and its demands or impacts are attributed to the primary use; however, the burdens for collection and separation of postconsumer waste polyethylene have been included.(*5*) Direct energy inputs for the FJH process were measured experimentally (Figure S27), and cumulative demands and impacts were calculated using Argonne National Laboratory GREET life-cycle assessment. Direct comparison of our life-cycle assessment with other literature values is possible if all databases utilized (*e.g*. GREET, SimaPro, Ecoinvent, and Gabi) follow International Standards Organization best standard procedures. Literature values presented in this discussion all comply with this requirement.

Key assumptions used when conducting the FJH and FeAlOx/microwave LCAs herein include that the power source for these methods, like with green hydrogen electrolysis, is renewable energy, and that thus no emissions or water use are contributed from powering each method. The amount of greenhouse gases emitted is thus a result of sourcing and preparation of materials and any CO_2 produced stoichiometrically by the process. A sale price of US$16,000 per ton is assumed for the MWCNT, as significant purification will be required to remove the reported ~10-30 wt% of catalyst. A 'worst case' scenario is assumed for the sale price of graphene, at US$3,000 per ton, to account for possible market saturation. This assumed sale price of graphene at US$3,000 per ton is 95% lower than actual current market value of multi-layered graphene products (US$60,000 per ton). Cost of post-consumer HDPE was considered in the technoeconomic analysis. An estimated overhead costs of capital expenses and operating expenses was based on averages of work done by Lan and Yao for 2000 tons of plastic processed per day basis factory ($1.20 per kg H_2)(*6*), as well as work done by the National Renewable Energy Labs for 500 tons of biomass processed per day basis factory ($3.10 per kg H_2)(*7*). Overhead costs can be accurately modelled using software such as Aspen Plus, but this was deemed beyond the scope of this current work. Further LCA details and scenarios are presented in Figure S11 and Table S2.

Computational Methods

The initial configuration of the atomistic model of HDPE particles was created by generating one carbon chain at a time, where each chain was composed of straight and curved segments of random length between 3 and 8 carbon atoms and curved segments displaying deviation from the straight line in randomized direction with angle up to 60° per carbon atom. The direction of the polymer chains was adjusted if the distance to any chain was found to be lower than 3.4 Å. Any chain shorter than 150 atoms was discarded to prevent structural unraveling during

molecular dynamics (MD) simulation. Hydrogen atoms were iteratively added after all carbon chains were generated. The final structure contained ~16,000 atoms. To allow the generation of H2 and other gases, the periodic box significantly exceeded the size of the HDPE particle and was set to 300 Å in all directions.

The MD simulations were carried out with AIREBO interatomic potential,(*8*, *9*) as implemented in the LAMMPS package.(*10*) To eliminate any possible artifacts introduced during structure creation, the initial configuration was subjected to geometric optimization followed by the annealing at 400 K for 5 × 10-9 s. The structure was then heated to target temperatures (1500 K and 3000 K) with the heating speed of 0.5 × 10-12 Ks-1 using a Nose–Hoover thermostat (canonical NVT ensemble) with a temperature damping parameter of 0.025 × 10-12 s and was held at the target annealing temperatures for 20 × 10-9 s.

Supplemental Figures:

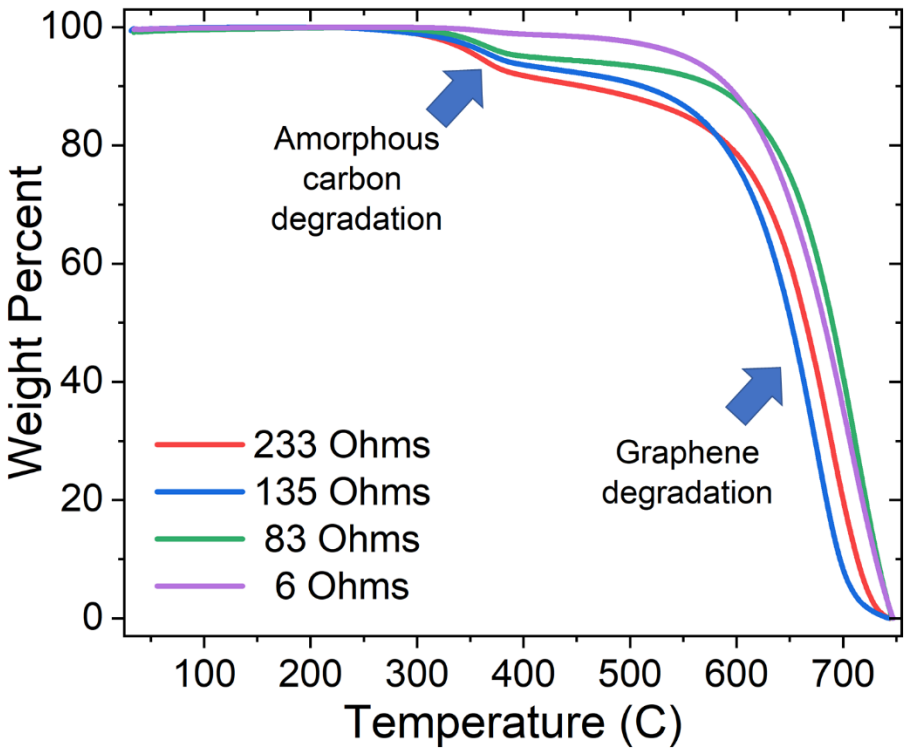

Figure S3. TGA under air atmosphere of produced solid carbon byproduct, as a function of initial sample resistance (air, 80 mL/min, heated at 5 °C/min).

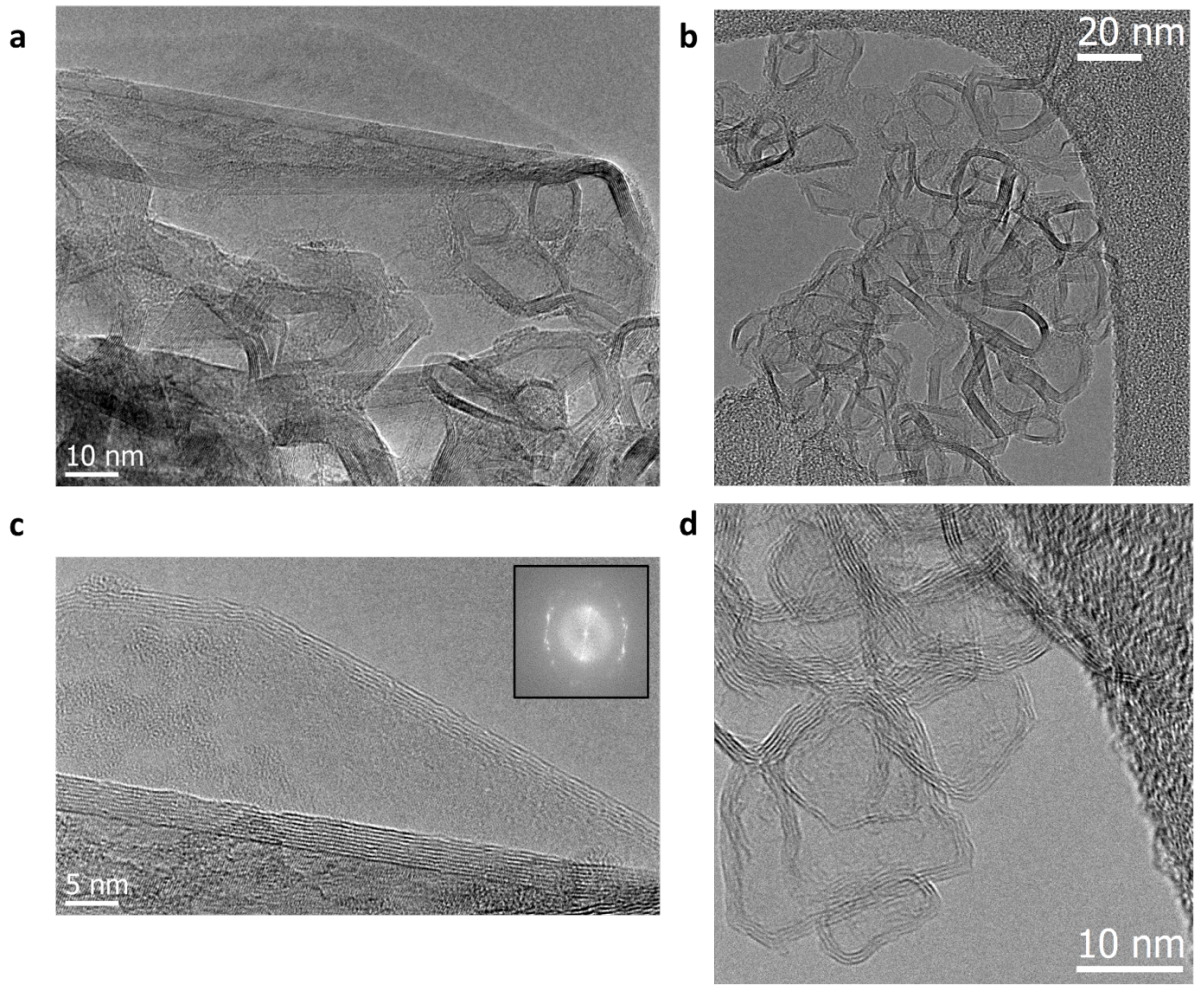

Figure S4. TEM images of the produced solid carbon from a sample of 6 Ohm initial resistance HDPE and carbon black. High resolution TEM (c) shows Moiré patterns of the turbostratic graphene, as further demonstrated by the inset fast Fourier transform (FFT).

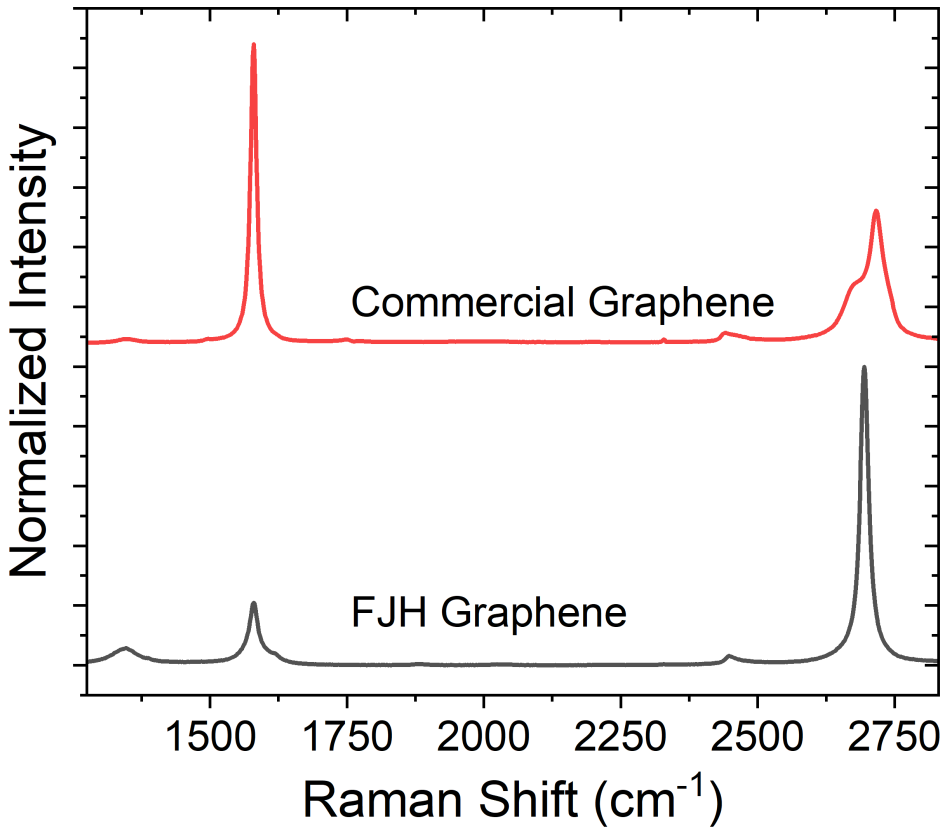

Figure S5. High resolution Raman spectra comparing graphene resulting from FJH of a sample of 6 Ohm initial resistance HDPE and carbon black, with commercially available graphene.

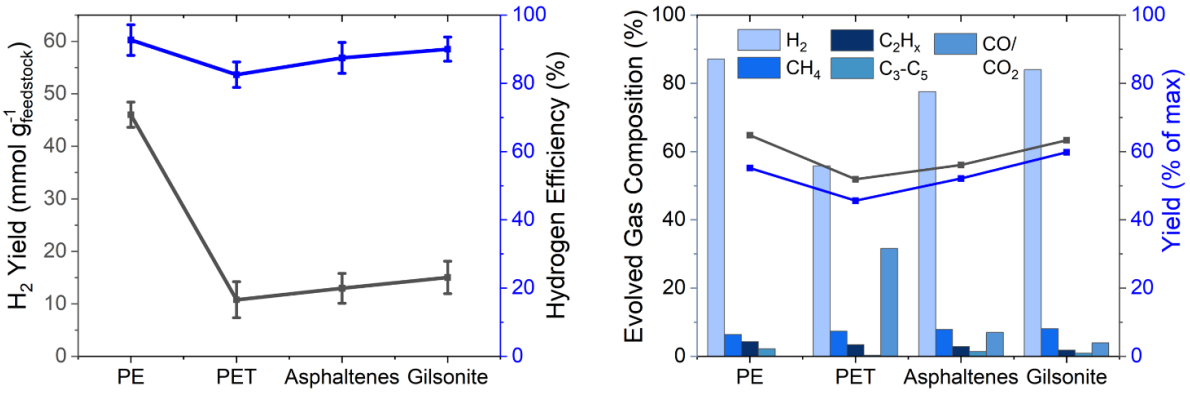

Figure S6. The FJH conversion of asphaltenes to H_2 and graphene demonstrating high yield, efficiency, and purity of gas stream as well as high quality graphene. This sample was heated at 6 ohms.

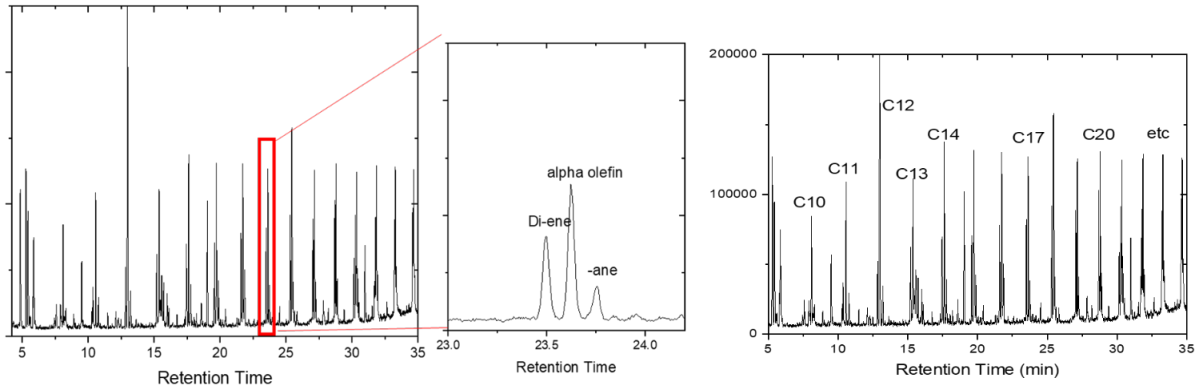

Figure S7a. Chromatogram showing alpha olefins to be the predominant oil and wax product produced from the FJH of polyethylene. The FJH process occurs orders of magnitude faster than traditional pyrolytic processes. The FJH of HDPE results in sizeable amounts of alpha-olefin gases, oils, and waxes, supporting a homolytic deconstruction mechanism.

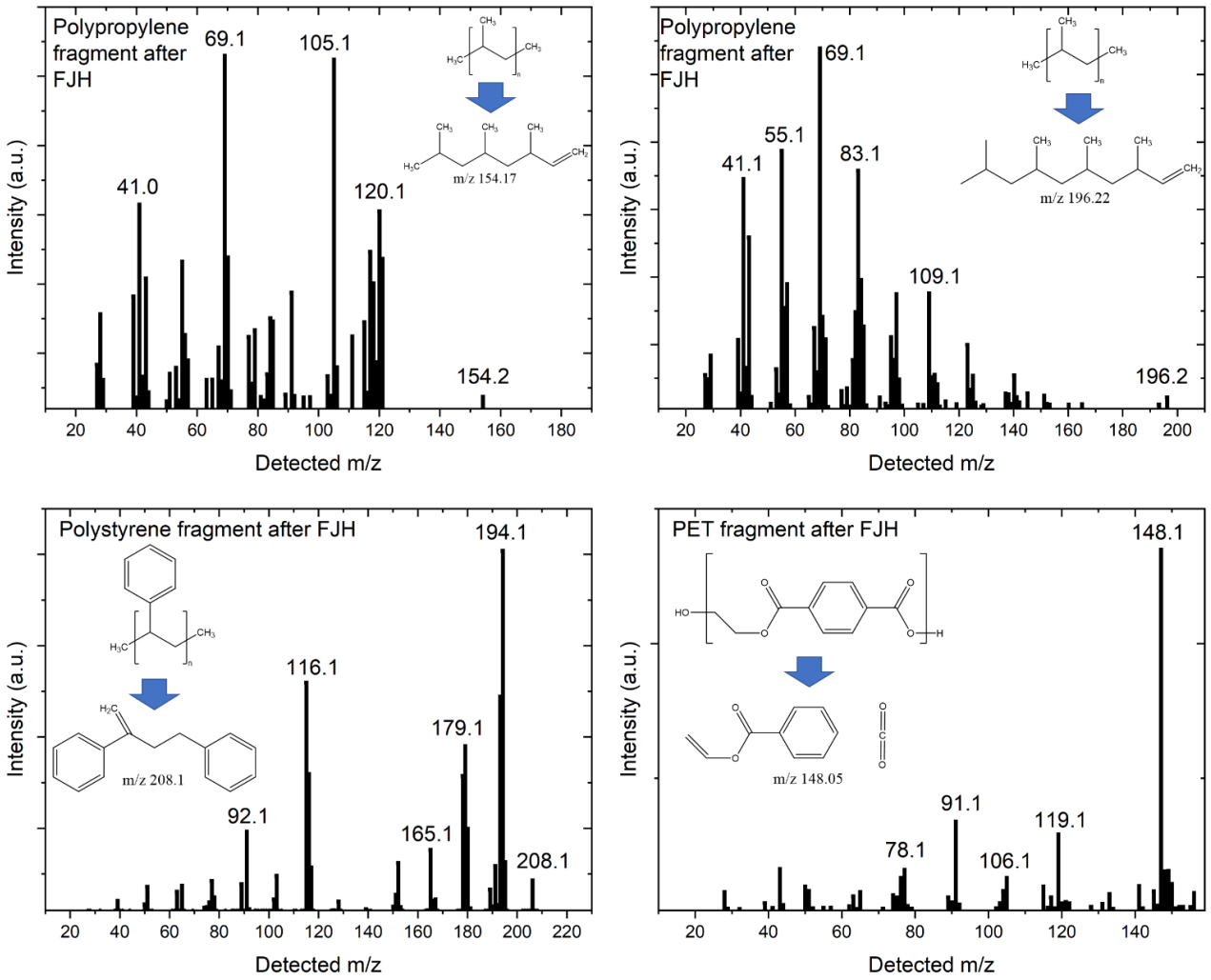

Figure S7b. Example mass spectra of fragments resulting from the FJH of various polymers showing that fragments of the parent polymer can be observed.

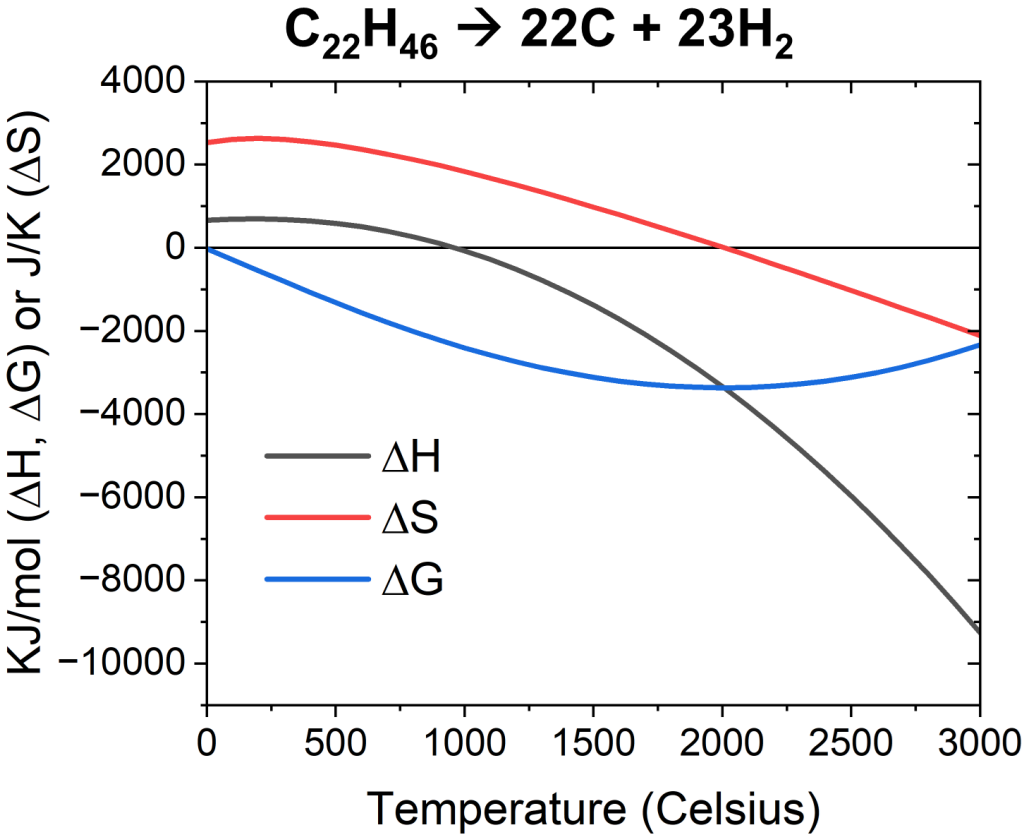

Figure S8. Thermodynamic calculations (HSC Chemistry, Version 9) studying the catalyst-free reaction pathway of a polyethylene adduct as a function of reaction temperature. Note that the enthalpy of reaction does not become negative until above 1,000 C, explaining why H_2 evolution is not observed during traditional low temperature, slow heating rate pyrolysis processes.

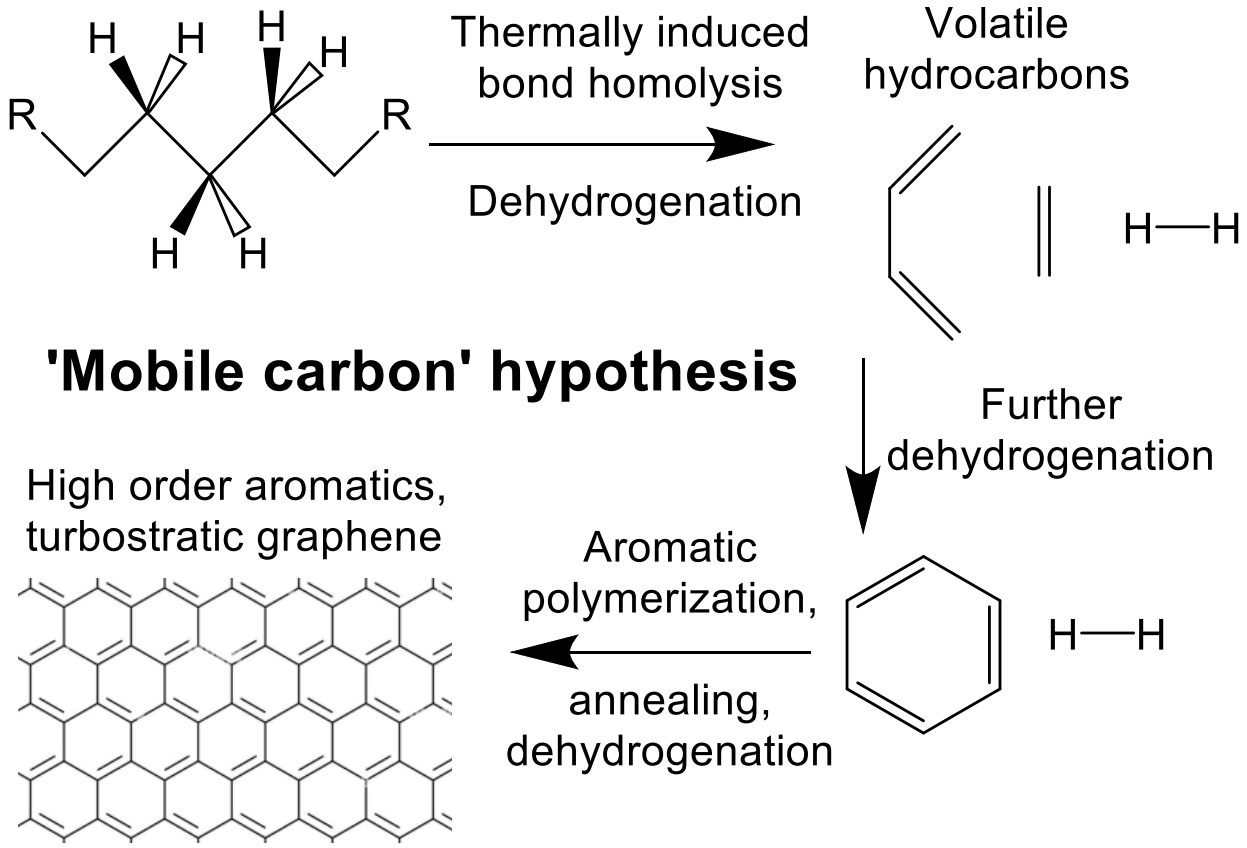

Figure S9. A diagram showing a possible mechanism for the formation of graphene and H_2 from HDPE.

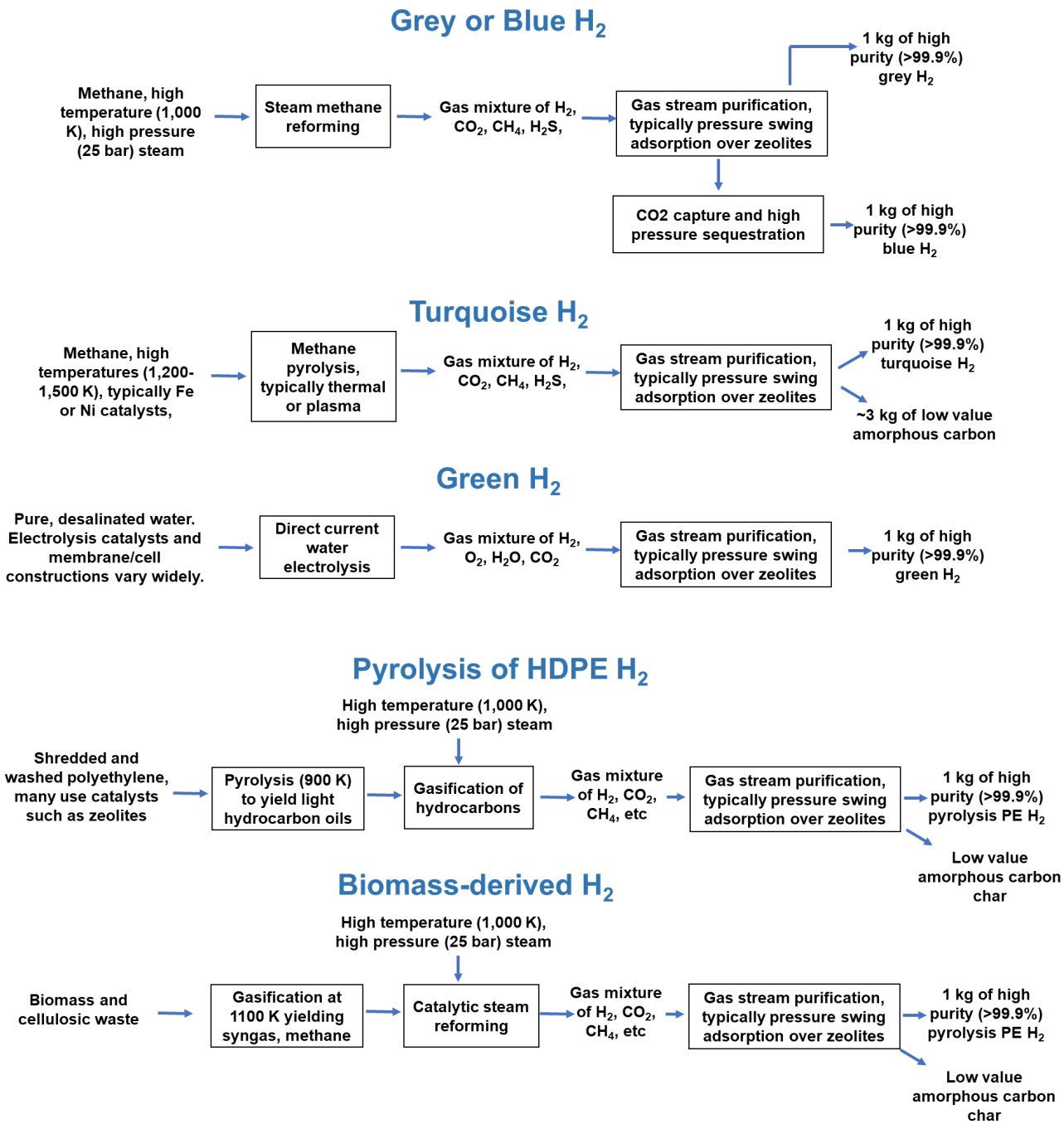

Figure S10. Simplified cradle-to-gate life-cycle inventories for the production of H_2 from traditional methods.

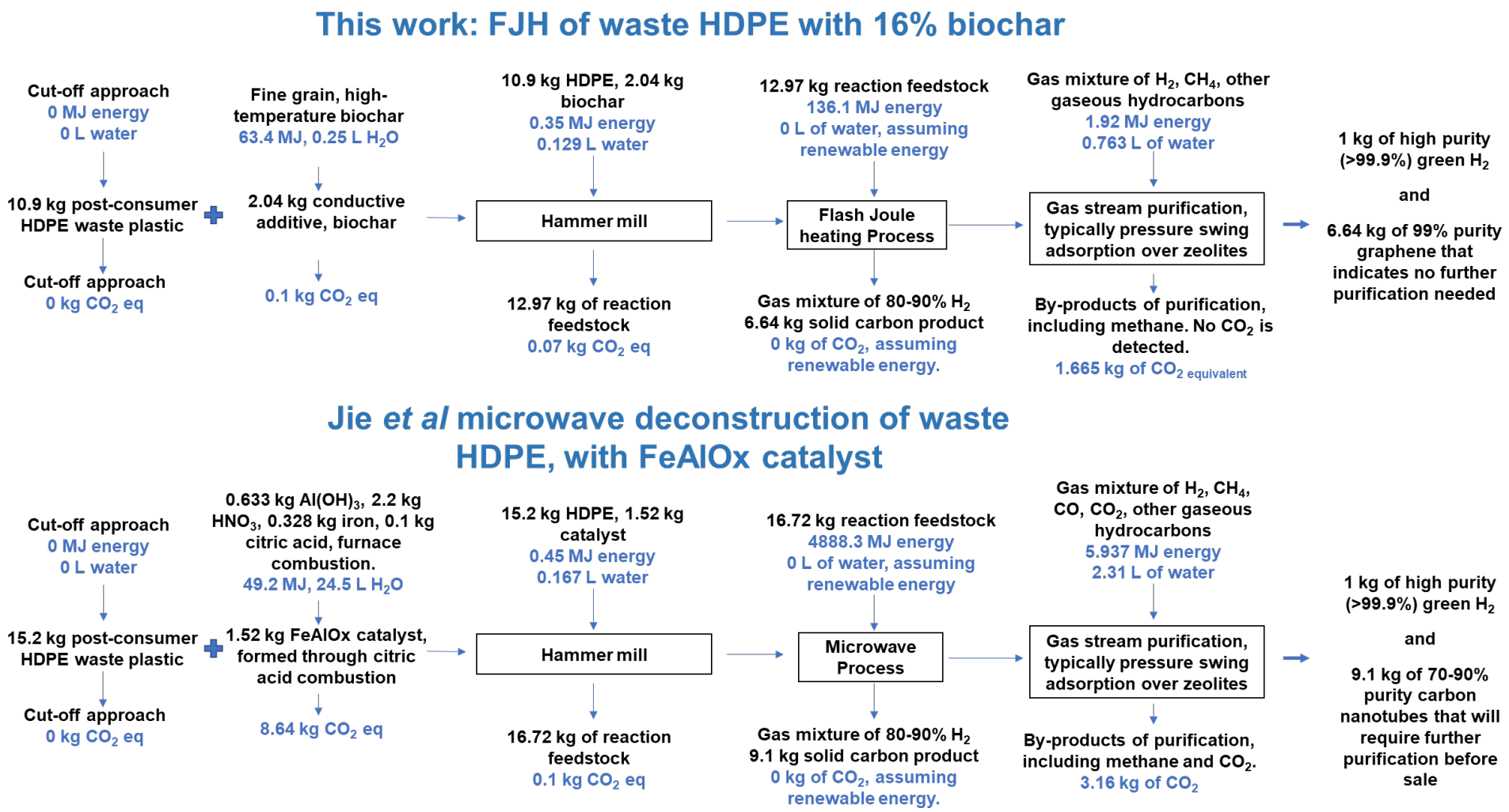

Figure S11. Complete cradle-to-gate life-cycle inventories for the FJH of plastic and for the catalyst-assisted microwave deconstruction of HDPE.

	Cumulative Energy Demand (MJ per kg H2)	Source	Global Warming Potential (kg CO2 eq per kg H2)	Source	Hydrogen Production Cost (USD$ per kg H2)	Source
Green Hydrogen	210	GREET	0.88	Hermesmann and Mueller, *Prog. Energy Combust.Sci.* , **2022**, 90, 100996.	4.8	Ajanovic, Sayer, Haas, *Int. J. Hydrog. Energy,* **2022**, 47, 24136.
Grey Hydrogen	135	Cetinkaya, Dincer, Naterer, *Int. J. Hydrog. Energy,* **2012**, 37, 2071.	11.57		1.67	
Blue Hydrogen	165	Ingale et al, *Energies* , **2022**, 15, 8679.	3.97		2.85	
Turqouise Hydrogen	240		3.01		2.05	Arcos and Santos, *Gases,* **2023**, 3, 25.
Flash Joule heating	201.7	**This work**	1.83	**This work**	-4.243	**This work**
Microwave and FeAlOx catalyst	4943	**This work**	10.73	**This work**	3.446	**This work**
Plastic Pyrolysis and reforming	298	Chari *et al* , *ACS Sustainable Chem. Eng.,* **2023**, 11, 3248.	16.1	Lan and Yao, *Commun. Earth Environ.* , **2022**, 3, 300	2.94	Lan and Yao, *Commun. Earth Environ.* , **2022**, 3, 300
H2 from Biomass gas	406	GREET	5.2528	GREET	3.1	M. Ruth and the National Renewable Energy Lab (NREL), **2011**, Hydrogen Production Cost Estimate Using Biomass Gasification: Independent Review. Report Number: NREL/BK-6A10-51726

Table S1a. A table showing the literature values and sources of values used in Figure 5f-h.

Amount of catalyst used	Method	Reforming?	Catalyst used	Amount recovered (mmol of atomic hydrogen per g feedstock)	Reference
	Theoretical maximum in HDPE			71.4 mmol	Theoretical maximum
0%	Flash Joule heating, no reforming	**NONE**	**NONE**	46.59 mmol	This work
0%	Two stage pyrolysis	**NONE**	**NONE**	8.08 mmol	*Appl. Catal. B.,* 2018
33%	Two stage pyrolysis	**NONE**	2:1 FeNiAlO	31.8 mmol	
33%	Traditional Pyrolysis	**NONE**	Ni-La/AlO	15.2 mmol	*Catalyts,* 2022
0%	Traditional Pyrolysis	Yes	**NONE**	3.04 mmol	*J. Energy Inst.* , 2021
71%	2/1/4 mixture of plastic/Ce-Ni-Zeloite catalyst/dolomite, pyrolysis, reforming	Yes	Ce-Ni Zeolite	11.4 mmol	
33%	Same, no dolmite	Yes	Ca/Mg/NI/Ce	10.2 mmol	

Table S1b. A table showing the literature values and sources of values used in Figure 5i comparing the production of H_2 from waste materials. (Continued on next page)

Amount of catalyst used	Method	Reforming?	Catalyst used	Amount recovered (mmol of atomic hydrogen per g feedstock)	Reference
50%	Traditional Pyrolysis	**NONE**	1:1 FeAlO	4.3 mmol	*Nature Catal .*, 2020
50%	Microwave Pyrolysis	**NONE**	1:1 FeAlO	55.6 mmol	
50%	Plasma pyrolysis	Yes	Ni/AlO	4.56 mmol	*ACS Energy Fuels* , 2020
59%	Plasma pyrolysis	Yes	MCM-41 Zeolite	18 mmol	*ACS Energy Fuels* , 2022
59%	Plasma pyrolysis	**NONE**	MCM-41 Zeolite	11 mmol	
33%	Two stage pyrolysis	**NONE**	FeNi solgel	9 mmol	*Chem Eng J, 2022*
29%	Two stage pyrolysis	**NONE**	FeSiO	25.6 mmol	*J Anal Appl Pyrolysis* , 2017
33%	Two stage pyrolysis	**NONE**	1:2 FeAlO	19.1 mmol	*Appl. Catal. B.*, 2016
33%	Two stage pyrolysis	**NONE**	1:2 NiAlo	11.7 mmol	
33%	Two stage pyrolysis	**NONE**	1:2 NiFeAlO	36.2 mmol	*Energy Convers. Manag.* 2017
1%	nIR photo dehydrogen	None	PtTi	26.19 mmol	Nature Energy 2022
50%	Microwave Pyro	none	1:1 FeAlO	48.1 mmol	Processes 2022

Table S1b. A table showing the literature values and sources of values used in Figure 5i comparing the production of H_2 from waste materials.

Catalyst-free deconstruction of waste HDPE into hydrogen and graphene, by flash Joule heating. The current work demonstrates that 46.59 mmol of hydrogen is produced per g of HDPE when a mixture of postconsumer HDPE and conductive additive undergoes flash Joule heating. No catalyst is needed. To produce 1 kg of hydrogen, 10.94 kg of HDPE and 2.04 kg of conductive additive are required. This will also produce 6.64 kg of turbostratic grapene.											
Raw inputs	Unit	Material/Process	Cumulative Energy Demand (CED) MJ/unit	100 Year Global Warming Potential (kg CO2 /unit)	Cumulative Water Use (L/ unit)	Material (M) or Process (P)	Cumulative Energy Demand (CED) MJ	100 Year Global Warming Potential (kg CO2 equivalent)	Cumulative Water Use (L)	Notes	Reference
Catalyst free flash Joule heating											
Preparing reaction mixture											
10.934	kg	Post consumer HDPE	-	-	-	M	-	-	-	Burdens disregarded, attributed to primary use, 'cut-off' approach	-
2.04417	kg	Conductive additive, assumed to be biochar	31	0.048	0.124	M	63.36927	0.09812016	0.25347708		GREET
12.97817	kg	Hammer milling	0.027	0.005	0.01	P	0.350411	0.069952336	0.1297817	To homogeneously mix catalyst and plastic, requires 0.027 MJ/kg	Bortnowski, P.; Gładysiewicz, L.; Król, R.; Ozdoba, M. Energies 2021, 14 (6), 1786.
Flash Joule heating reaction											
12.97817	kg	Reaction feedstock	-	-	-	M	-	-	-	Tabulated above.	-
25552	Reaction iterations	Flash Joule heating	0.005324	0.0011175	0.002071	P	136.0388	28.5545542	52.91911187	The reaction feedstock is processed in batches of 0.5 g. This requires 25552 reaction iterations to process 12.97 kg of precursor. The experimentally determined energy input was found to be 5.234 kJ per reaction iteration.	GREET, using US central plains energy mix
Gas Purification											
3.1147608	kg gas to purify	Pressure swing adsorption for gas capture and	0.63	0.1243	0.245	P	1.962299	0.387164767	0.763116396	Pressure swing adsorption purification of total gas stream	GREET
Process Outputs											
1	kg	Hydrogen gas	-	-	-	M	-	-	-		-
6.64	kg	multiwalled carbon nanotubes	-	-	-	M	-	-	-	Pure product by XPS and TGA, indicating no further purification needed before sale	-
25552	Reaction iterations	Other gases	-	0.00005	-	M	-	1.2776	-	Minor contributions of methane 0.00005 kg (evolved per reaction iteration, combusted to offset FJH energy demand	-
							CED	**GWP**	**CWU**		
						Assuming Fossil Fuels	**201.72**	**30.38739**	**54.065487**		
						Assuming Renewable Energy	**201.72**	**1.832837**	**1.1463752**		

Table S2a. Table of considered values for the preliminary LCA studying the flash Joule heating method.

Deconstruction of waste HDPE into hydrogen and (predominantly) carbon nanotubes, by FeAlOx catalyst-assisted microwave heating. Work by Jie *et al* show that over 10 catalytic cycles, an average of 33 mmol of hydrogen is produced per gram of HDPE and gram of catalyst used. To produce 1 kg of hydrogen, 15.2 kg of HDPE and 1.52 kg catalyst are required, assuming 10 catalytic cycles. This will also produce 9.1 kg of multiwalled carbon nanotubes.											
Raw inputs	Unit	Material/Process	Cumulative Energy Demand (CED) MJ/unit	100 Year Global Warming Potential (kg CO2 eq/unit)	Cumulative Water Use (L/ unit)	Material (M) or Process (P)	Cumulative Energy Demand (CED) MJ	100 Year Global Warming Potential (kg CO2 equivalent)	Cumulative Water Use (L)	Notes	Reference
Microwave and FeAlOx catalyst											
Synthesizing 1.52 kg of the Catalyst				1:1:1 citric acid/iron nitrate/aluminum nitrate molar ratio as specified by Jie et al. The mass yield of catalyst product after citric acid combustion synthesis is 65%. Thus, 2.34 kg precursor required to form 1.52 kg catalyst. This requires							
0.633	kg	Aluminum Hydroxide	8.058	0.6446	6.106	M	5.100714	0.4080318	3.865098	To synthesize 1 mol aluminum nitrate (0.213 kg). 2 mol Al(OH)3, or 0.166 kg salt, required and 3 mol fuming nitric acid, or 0.189 kg acid.	GREET
0.720704819	kg	Nitric Acid	7.427	1.4056	3.636	M	5.352674693	1.013022694	2.62048272		GREET
0.328	kg	Iron Ore	0.538	0.0458	0.059	M	0.176464	0.0150224	0.019352	To synthesize iron nitrate (0.242 kg). 1 mole of iron ore, or 0.0558 kg ore, required and 4 mol fuming nitric acid, or 0.252 kg acid.	GREET
1.481290323	kg	Nitric Acid	7.427	1.4056	3.636	M	11.00154323	2.082101677	5.38597161		GREET
102.2	g	Citric Acid	0.0368	0.001482	0.0272	M	3.76096	0.1514604	2.77984	-	GREET
0.56	kg	Water	-	-	1	M	-	-	0.56	Minimal water to form gel phase.	GREET
3	hr	Furnace Combustion	7.92	1.66	3.08	P	23.76	4.98	9.24	350C for 3 hours. 2.2 kW per hour.	-
Reaction Feedstock											
15.2	kg	Post consumer HDPE	-	-	-	M	-	-	-	Burdens disregarded, attributed to primary use, 'cut-off' approach	-
1.52	kg	FeAlOx catalyst	-	-	-	M	-	-	-	Tabulated above.	-
16.72	kg	Hammer milling	0.027	0.005	0.01	P	0.45144	0.0901208	0.1672	To homogeneously mix catalyst and plastic, requires 0.027 MJ/kg	Bortnowski, P.; Gładysiewicz, L.; Król, R.; Ozdoba, M. Energies 2021, 14 (6), 1786.
Microwave Reaction											
50667	Reaction iterations	Microwave reaction	0.09648	0.0196	0.035	P	4888.35216	993.0732	1773.345	Jie et al used 1000 W microwave (2,400 MHz) for 90 seconds. An efficency of 93% is provided by the authors. This is equivalent to 0.0268 kWh per 0.0003 kg HDPE deconstructed. This results in 50,667 reactions required to process 15.2 kg plastic.	GREET, using US central plains energy mix
Process Outputs											
9.424	kg gas to purify	Pressure swing adsorption purification	0.63	0.1243	0.245	P	5.93712	1.1714032	2.30888	Pressure swing adsorption purification of total gas stream	GREET
Process Outputs											
1	kg	Hydrogen gas	-	-	-	M	-	-	-		-
9.1	kg	multiwalled carbon nanotubes	-	-	-	M	-	-	-	70-90% purity carbon nanotubes that will require further purification before sale	-
50667	Reaction iterations	Other gases	-	3.93216E-05	-	M	-	1.992307507	-	Minor quantities of other gases (methane, carbon monoxide, carbon dioxide) are produced concurrently during the reaction. Jie et al report tha, on average, methane makes up 6.52% of the gases produced and CO2 makes up 0.84% of the gases.	-
							CED	**GWP**	**CWU**		
						Assuming Fossil Fuels	**4943.893**	**1004.97667**	**1797.98**		
						Assuming Renewable Energy	**4943.893**	**10.73206728**	**26.9468**		

Table S2b. Table of considered values for the preliminary LCA studying the microwave deconstruction method by Jie *et al* (*11*).

Microwave deconstruction of HDPE with FeAlOx Catalyst					
Amount	**Unit**	**Material**	**Cost/unit**	**Total**	**Source**
Inputs					
0.633	kg	Aluminum Hydroxide	0.45	0.28485	2022 industrial market price
0.720705	kg	Nitric Acid	0.285	0.205401	2022 industrial market price
0.328	kg	Iron Ore	0.12	0.03936	2022 industrial market price
1.48129	kg	Nitric Acid	0.285	0.422168	2022 industrial market price
102.2	g	Citric Acid	0.022	2.2484	2022 industrial market price
15.2	kg	Post consumer HDPE	0.48	7.296	Lan and Yao, *Commun. Earth Environ.* , **2022**, 3, 300
1364	kWh	Electricity	0.1	136.4	2022 industrial market price, West TX, USA
1	cost per 1 kg H2	Overhead, including operating costs, labor, and PSA purification.	2.15	2.15	Lan and Yao, *Commun. Earth Environ.* , **2022**, 3, 300
Outputs					
9.1	kg	MWCNT	-16	-145.6	Projected profit
1	kg	Hydrogen Gas	-	3.446	Net **cost** assuming MWCNT sale

Flash Joule heating of HDPE with biochar additive					
Amount	**Unit**	**Material**	**Cost/unit**	**Total**	**Source**
Inputs					
2.044	g	Biochar	1.85	3.7814	Nematian, Keske, and Ng'ombe, *Waste Management,* **2021**, 135, 467.
10.934	kg	Post consumer HDPE	0.48	5.24832	Lan and Yao, *Commun. Earth Environ.* , **2022**, 3, 300
44.97	kWh	Electricity	0.1	4.497	2022 industrial market price, West TX, USA
1	cost per 1 kg H2	Overhead, including operating costs, labor, and PSA purification.	2.15	2.15	Lan and Yao, *Commun. Earth Environ.* , **2022**, 3, 300
Outputs					
6.64	kg	Graphene	-3	-19.92	Projected profit
1	kg	Hydrogen Gas	-	-4.243	Net **profit** assuming graphene sale

Table S3. Table of considered values, and accompanying sources, for the TEAs conducted.

Supplemental References:

1. D. X. Luong, K. V. Bets, W. A. Algozeeb, M. G. Stanford, C. Kittrell, W. Chen, R. V. Salvatierra, M. Ren, E. A. McHugh, P. A. Advincula, Z. Wang, M. Bhatt, H. Guo, V. Mancevski, R. Shahsavari, B. I. Yakobson, J. M. Tour, Gram-scale bottom-up flash graphene synthesis. *Nature*. **577**, 647–651 (2020).

2. K. M. Wyss, Z. Wang, L. B. Alemany, C. Kittrell, J. M. Tour, Bulk Production of Any Ratio 12C:13C Turbostratic Flash Graphene and Its Unusual Spectroscopic Characteristics. *ACS Nano*. **15**, 10542–10552 (2021).

3. K. M. Wyss, D. X. Luong, J. M. Tour, Large-Scale Syntheses of 2-D Materials: Flash Joule Heating and Other Methods. *Adv. Mater.* **n/a**, 2106970.

4. W. A. Algozeeb, P. E. Savas, D. X. Luong, W. Chen, C. Kittrell, M. Bhat, R. Shahsavari, J. M. Tour, Flash Graphene from Plastic Waste. *ACS Nano*. **14**, 15595–15604 (2020).

5. M. A. Martín-Lara, J. A. Moreno, G. Garcia-Garcia, S. Arjandas, M. Calero, Life cycle assessment of mechanical recycling of post-consumer polyethylene flexible films based on a real case in Spain. *J. Clean. Prod.* **365**, 132625 (2022).

6. K. Lan, Y. Yao, Feasibility of gasifying mixed plastic waste for hydrogen production and carbon capture and storage. *Commun. Earth Environ.* **3**, 1–11 (2022).

7. N. T. Contact, M. Ruth, Hydrogen Production Cost Estimate Using Biomass Gasification: Independent Review.

8. S. J. Stuart, A. B. Tutein, J. A. Harrison, A reactive potential for hydrocarbons with intermolecular interactions. *J. Chem. Phys.* **112**, 6472–6486 (2000).

9. D. W. Brenner, O. A. Shenderova, J. A. Harrison, S. J. Stuart, B. Ni, S. B. Sinnott, A second-generation reactive empirical bond order (REBO) potential energy expression for hydrocarbons. *J. Phys. Condens. Matter*. **14**, 783 (2002).

10. A. P. Thompson, H. M. Aktulga, R. Berger, D. S. Bolintineanu, W. M. Brown, P. S. Crozier, P. J. in 't Veld, A. Kohlmeyer, S. G. Moore, T. D. Nguyen, R. Shan, M. J. Stevens, J. Tranchida, C. Trott, S. J. Plimpton, LAMMPS - a flexible simulation tool for particle-based materials modeling at the atomic, meso, and continuum scales. *Comput. Phys. Commun.* **271**, 108171 (2022).

11. X. Jie, W. Li, D. Slocombe, Y. Gao, I. Banerjee, S. Gonzalez-Cortes, B. Yao, H. AlMegren, S. Alshihri, J. Dilworth, J. Thomas, T. Xiao, P. Edwards, Microwave-initiated catalytic deconstruction of plastic waste into hydrogen and high-value carbons. *Nat. Catal.* **3**, 902–912 (2020).